

Building the Digital Twin of Existing Highway Using Map Data Based on the Engineering Expertise

Feng Jiang [a], Ling Ma [a], Tim Broyd [a], Weiya Chen [b], Hanbin Luo [b]
[a] The Bartlett School of Construction and Project Management, University College London, London WC1E 6BT, UK
[b] School of Civil Engineering and Mechanics, Huazhong University of Science & Technology, Wuhan 430074, China

ABSTRACT

Highway asset management requires capturing the highway's status. However, the onsite survey of the highway is very costly and time-consuming. This paper presents a novel approach for creating the digital twin of a highway using map data. The digital twin consists of primary highway components, including horizontal alignment, vertical alignment, cross-section, lanes and central reserves. It follows the engineering representation of a highway, which has excellent potential for further application in the field. The proposed approach was tested in a section of the A1(M) motorway in the UK. It requires minimum human input and has very high accuracy. Despite many outliers in the collected map data, the average vertical deviation per square metre between the surface of the generated digital twin and the actual data was at the centimetre level.

Keywords: Digital Twin; Highway engineering; Alignment fitting; Cross-section; Map; Point clouds; Arial photograph

1 INTRODUCTION

Many roads have been constructed in the past decades and serve society to promote transportation and economic development. According to the statistics, the overall length of the road is 64,285,009km in 2013. In 2019, there are 6,853,02km roads in the United States, including 95,932km expressways, and there are 5,012,500km roads in China, including 149,600 km expressway [45]. These vast numbers bring people's attention to the existing road. People always need to do something with existing roads, such as road network planning, traffic simulation and analysis, operation and maintenance, reconstruction and expansion. Surrounding existing old road networks and the environment should be considered for road network planning [47]. For traffic simulation and analysis, the process needs to be operated on existing roads [26]. For road operation and maintenance, the analysis and evaluation should be based on the as-is roads, and the up-to-date status of the roads should be collected [35]. For reconstruction and expansion projects, the old road's data should be collected first, and then, the widen new road should be constructed based on the old road [39]. When people want to collect some existing data on old roads for different purposes, they may not find enough available materials due to missing or incomplete archives.

Also, many old roads were constructed without digital drawings [8]. Even if people can find some existing data, these data are usually paper drawings, pdf files, and some unstructured data. Grieves and Vickers [16] proposed that the Digital Twin is a set of virtual information constructs that fully describes a potential or actual physical manufactured product from the micro atomic level to the macro geometrical level. Any information obtained from inspecting a physically manufactured product can be obtained from its Digital Twin at its optimum. Thus, a digital twin can bring a high-fidelity digital replica to the road to solve these problems, and it also can provide integrated and structured data [38,43]. The digital twin has been implemented in the construction sector [5] from the manufacturing industry [22]. It is an effective tool for representing the existing old roads and their current status.

Generally, the digital twin consists of five parts: physical part, virtual part, connection, data, and service [41]. In the field of construction, digital twin, laser scanners, LiDAR devices, cameras and strain sensors are employed to collect geometric information from a target entity in the physical world to create digital twins [44], maintain existing buildings [2], detect bridges' defects [32], and many more. Also, sensors are employed to collect non-geometric information from a physical entity to its digital twin to realise asset management and monitoring [46]. However, most digital twin applications focus on structural entities rather than long-shape infrastructure. Additionally, some works that do not require high-precision road digital twin models, such as preliminary research and work, are too wasteful to employ some people and devices to collect data.

Moreover, considering some special conditions, such as bad weather, severe pandemic, limited time consuming and expenses allowed, the field survey is not appropriate to be conducted. Comparatively, some existing map databases are collected by satellites, rough LiDAR surveys, or even rough field surveys that can express the road's relatively up-to-date status [29]. However, the existing map data has a relatively low quality compared to the field survey data. For making a digital twin of an existing old road, several challenges should be considered:

1) How to make a digital twin for long-shape infrastructure?
2) How to make a digital twin following the representations used in road engineering domains, which consists of different road components (horizontal alignments, vertical alignments, cross-sections, wide variation, cross falls, lanes, central reserves, hard strips, shoulders, verges, side slopes and many more) and can be widely used in this field?
3) How to remove the defects caused by the relatively low quality and the limited survey condition of the downloaded map data? Generally, a field survey can be conducted according to the demands from different angles and at different

positions, while the map data such as satellite survey can only collect data from the top. Thus, overpasses, vegetations, shadows can influence the highway digital twin a lot.

4) How to remove the defects on the old road, such as pavement defects caused by vehicles and other factors, erosion of the side slopes, blurred boundaries between different road components and more?

This research proposed a novel approach that can build digital twins for existing old highways only based on existing map data. In Section 2, a background review of the digital twin in the construction sector is conducted. In Section 3, the proposed method is introduced, which consists of data acquisition and processing, horizontal alignment fitting, vertical alignment fitting, cross-section processing, and digital twinning. In Section 4, the digital twin of a section of the A1(M) highway is established using the downloaded map data from Digimap as a case study. Moreover, an evaluation method for the digital twin is proposed. Section 5 is the systematic discussion of the proposed method, and Section 6 concludes the research.

2 BACKGROUND

2.1 Digital twin in the construction sector

The digital twin is gradually implemented in the construction sector, especially in the operation and maintenance stage. Buildings can employ digital twins to monitor their conditions and control their environment. Kaewunruen and Xu [20] conducted a Revit-based simulation of construction work for King's Cross station in London using digital twin, which can convert the 3D model of the station building into a 6D building information model. The 6D model contains a time and cost schedule with carbon emissions calculation and renovation assumption. Lydon, et al. [30] presented a coupled simulation for a heating and cooling system's thermal design integrated with a lightweight roof structure based on digital twin. The concrete roof structure is shape optimised to provide a low embodied energy building element, thermally activated to supply space conditioning from a renewable geothermal source. Peng, et al. [34]developed a digital twin-based system with real-time visual management and artificial intelligent diagnosis modules to grasp the whole hospital's detailed status by visual management and receive timely facility diagnosis and operation suggestions, which are automatically sent back from the digital building to reality. The system can reduce energy consumption, avoid facility faults, reduce the number of requested repairs, and enhance daily maintenance work quality. Liu, et al. [25] established a digital twin multidimensional model of prestressed steel structures, which can be implemented in a large stadium. Based on this model, the support vector machine and prediction model were trained using the relevant structural history data, and the safety risk level of the structure was then predicted based on the measured data.

In the field of infrastructure, digital is implemented to bridges, tunnels, railways, roads for operation and maintenance. Lu and Brilakis [28] proposed a slicing-based object fitting method that can generate the geometric digital twin of an existing reinforced concrete bridge from four types of labelled point clusters and provided an evaluation method. Shim, et al. [40] proposed a digital twin-based bridge maintenance system to enhance the bridge maintenance process using a parallel solution: a maintenance information management system based on a 3D information model in conjunction with a digital inspection system using image processing for more reliable decision making. Ye, et al. [48] conducted a visual inspection, operational monitoring, forced excitation testing, controlled load testing, non-destructive probes, long-term monitoring, finite element modelling, parameter identification, and 3D DT development for a 30-year-old expressway bridge in New Jersey, which enabled them to determine the root causes of the multiple complex performance defects systematically. Lin, et al. [23] established design document-based, linearly updated, and nonlinearly updated FE models, to demonstrate the necessity of the digital twin-based assessment. Incremental dynamic analyses (IDA) are conducted to calculate the FE models' collapse fragility curves, and the assessment results are compared with the test results in terms of collapse mechanisms, collapse ground motion intensities, and collapse probabilities. Ariyachandra and Brilakis [3] proposed a method for detecting masts from airborne light detection and ranging (LiDAR) data by leveraging the highly regulated and standardised nature of railways. Yu, et al. [49] propose a performance prediction approach for highway tunnel pavements based on a digital twin and multiple time series stacking (MTSS).

2.2 Different data resources

For creating a digital twin, some devices usually are employed to collect data from target projects in the physical world to their digital twins. First and for most, laser scanners and LiDAR are employed to collect geometric information by point clouds from the physical world for digital twinning. Omer, et al. [32] proposed a novel method for bridge inspection that essentially digitalises bridges using LIDAR, and they can be later inspected in a virtual reality (VR) environment. Ariyachandra and Brilakis [3] proposed a method for detecting masts from airborne LiDAR data by leveraging the highly regulated and standardised nature of railways. Rausch and Haas [36] presented an approach for creating geometric agency within BIM by exploiting their parametric capabilities, the accuracy of 3D point clouds, and the dexterity of metaheuristics to realise a dynamic BIM capable of updating its geometry to match a 3D point cloud from a laser scanner.

Also, sensors are employed to collect non-geometric information from target projects in the physical world to their digital twins for monitoring. Böke, et al. [6] developed a cyber-physical system and digital twin for a building facade to realise automated adaptive functions, considering sun protection, ventilation and heating and cooling functions using a prototype for the automated adaptive facade, sensors, microcontrollers, WiFi and brokers, and actuators. Huynh and Nguyen-Ky [18] proposed a framework for the efficient development of an interoperable visualisation of a building digital twin through an intuitive interface which is a progressive web application (PWA), where valuable sets of building performance data from sensors are visualised, and a promptly communicable channel between owners/occupants and building system is delivered. Ritto and Rochinha [37] constructed a digital twin for a damaged structure where a discrete physics-based computational model is employed to investigate several damage scenarios using machine learning and sensors.

Finally, other tools, such as cameras and field survey, are employed to collect digital twin's data. Lu, et al. [27] developed a semi-automatic framework to establish a systematic, precise, and convenient digital twinning system based on images and CAD drawings. The system consists of three modules, including the building framework construction and geometry information extraction module, the building information complementary module, which is developed based on neuro-fuzzy systems (NFS) and image processing, and the information integration and IFC creation module.

2.3 Existing road digitalizition

Various approaches related to digitalising existing road have been proposed from different perspectives. Generally, a road can be expressed by horizontal alignment, vertical alignment, and cross-sections. For alignment fitting, Karamanou, et al. [21] developed software for the precise estimation of road horizontal and vertical geometric features, using the GPS/IMU data collected during the digital survey of road nets. Easa and Wang [10] presented an optimisation model for estimating continuous vertical alignments parameters, involving multiple parabolic vertical curves that best fit existing highway profile data using the least-squares method. Garach, et al. [15] presented an approximation method to reconstruct a road's geometry. They chose a variational cubic spline for curve fitting, computed this spline's curvature function, and approximated the curvature function using a polygonal function formed by trapezoids on the abscises axis. This allows the alignments in a road (straights, curves or clothoid) and their respective curvature values to be identified from an approximation point set given by its UTM coordinates obtained from field data.

Zhang, et al. [50] compared Lagrange interpolation fitting, least-squares fitting, cubic spline fitting, and HintCAD software fitting based on coordinates of stations of an existing road and found that cubic spline fitting can express the characters of the horizontal alignment better with more minor errors. Unlike current methods that represent road alignment through its curvature, Camacho-Torregrosa, et al. [7] proposed a method describing the horizontal alignment as a sequence of headings to fit the horizontal alignment of a road to a set of (x, y) points that can be obtained from digital imagery or GPS-data collection. For cross-section, Holgado-Barco, et al. [17] proposed a method to obtain the geometrical inventory of road cross-sections using a mobile laser scanning (MLS) system. However, MLS's data quality is much better than the downloaded map data, and side slope modelling is not considered. Besides, they have not established an integrated 3D digital twin model for the highway. There is research related to existing pavement digitalisation for the pavement to assist in defects detection and maintenance. For example, Biçici and Zeybek [4] proposed an approach to automatically detect and measure road distress from images captured by unmanned aerial vehicles (UAV). This kind of research only focuses on the pavement. For overall existing road recognition, Liu and Lim [24] presented a new framework of road feature extraction from colour component-based data fusion of aerial imagery and lidar data. Jasim [19] extracted urban roads from DEM of LiDAR with IKONOS images using machine learning (ML). These two papers only can realise the road recognition and determine the positions of simple road lines without considering the road components. The results are not represented in the language of road engineering. Also, they did not make a digital twin for the road.

2.4 The gaps from the background

Several gaps are existing according to the literature review:

1) According to Section 2.1, from the perspective of target projects in the physical world, most existing construction digital twins are related to structures that can be regarded as "blocks". However, very few studies are related to long-shape infrastructures such as railways, tunnels, roads, which are constructed and adhere to the terrains, and they focus on the structures or pavement on the target project without considering the relationship with the terrain, such as the side slops. None of these studies is related to systematic digital twinning for a highway, considering its different components and the terrain.

2) According to Section 2.2, from the perspective of the connections and data resources, most existing digital twins collect data using some devices such as laser scanners, LiDAR, cameras or based on CAD drawings. None of them is based on existing map data.

3) According to Section 2.3, from the perspective of the digital twinning methods, first, most studies only consider part of the road elements, such as the alignment, the pavement, or the cross-section. Second, most existing road digital twinning methods are based on relatively high-quality data. Third, most studies related to road recognition and extraction are not represented in a way that road engineers use in the field. Fourth, none of them has made a 3D digital twin for a highway considering its elements (such as horizontal alignments, vertical alignments, cross-sections, wide variation, cross falls, lanes, central reserves, hard strips, shoulders, verges and side slopes) from the perspective of the road engineering expertise using downloaded map data.

3 THE APPROACH TO MAKE A DIGITAL TWIN FOR A HIGHWAY

The proposed approach consists of five steps, as shown in Fig. 1. The overall digital twinning process is from the perspective of highway engineering expertise. Some conditions and constraints following professional highway engineering knowledge and highway design standards can be inferred and used during the process to assist in digital twinning based on the map data with relatively low quality.

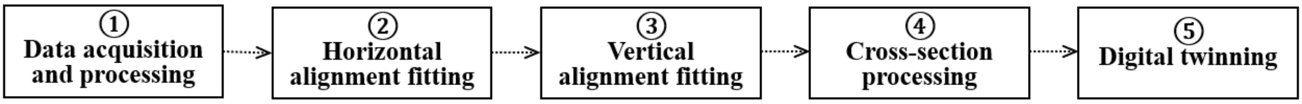

Fig. 1. The overall workflow for highway digital twin

3.1 Data acquisition and processing

Instead of obtaining data in the field, various forms of map data can be downloaded online, such as aerial photography, digital surface model (DSM), digital elevation model (DEM), topographies and more from different kinds of map downloading platforms and software. In this research, aerial photography data, DSM data, topographies are downloaded from a downloading platform called Digimap [1,9]. The overall workflow is as shown in Fig. 2.

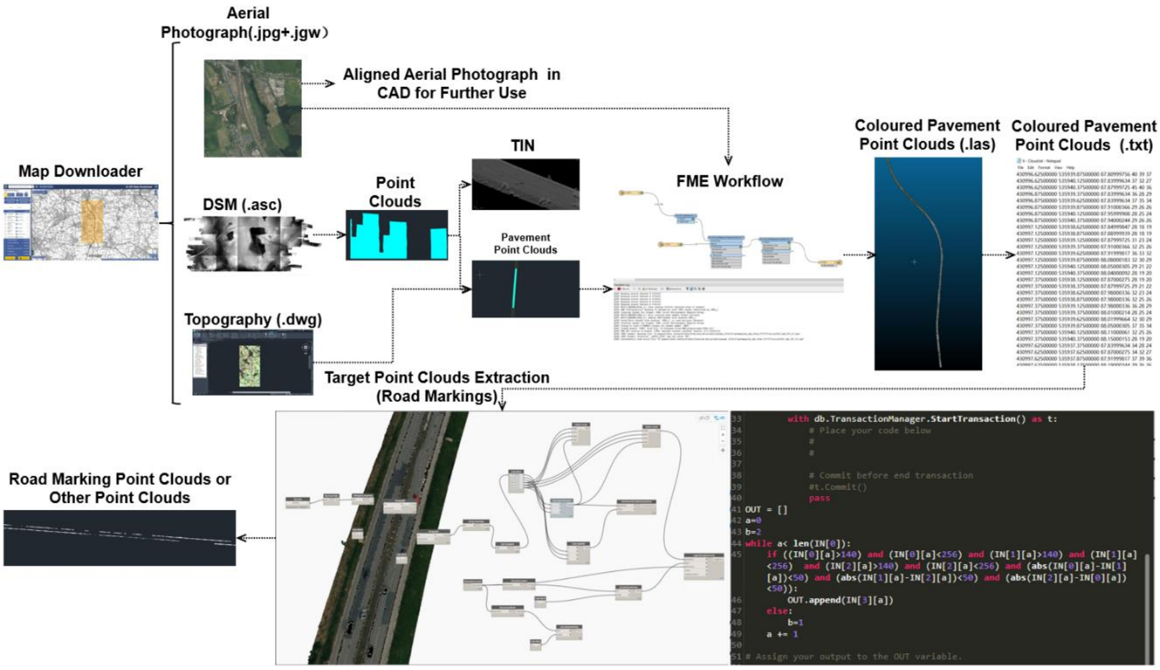

Fig. 2. Data acquisition and processing and road marking point clouds extraction

These data do not possess high precision as the data from field surveys has many defects. DSM or DEM data and aerial photography data are essential for basic digital twinning. However, topographies are not necessary to mark target areas roughly due to the low precision. Without topographies, aerial photography data can be implemented for marking areas roughly instead, after they are aligned with the right positions and scales in CAD. Thus, a closed polyline can be drawn to enclose the pavement scope. After that, the closed polyline can be offset outward to form a larger closed polyline called pavement polyline to enclose the pavement and some side slopes. DSM data are ASC format data converted to DEM in Civil 3D, and then point clouds are extracted from DEM. Afterwards, a TIN can be established using point clouds representing the target highway's scope, surrounding terrain, and surface features. The pavement polyline cuts the overall point clouds to get the highway's pavement point clouds with some side slope point clouds called pavement point clouds. Then, a flowgraph can be developed in FME software to combine aerial photography data in jpg and jgw format and pavement point clouds in dwg format together to form coloured pavement point clouds in las format. Due to the jgw documents, the aerial photography data can match the position of DEM and the point clouds very well. The coloured pavement point clouds in las format are converted to txt format documents in CloudCompare software, and each coloured point has six dimensions described as (x,y,z, R, G, B). The "x", "y", "z" represent positions and "R", "G", "B" represent the true colour "Red", "Green", and "Blue". Afterwards, all the points in the coloured pavement point clouds can be controlled and selected according to the six-dimensional coordinates using the txt format documents.

Road markings and edges of the pavement should be extracted by programming. For example, road marking point clouds are whiter and brighter than pavement point clouds. Thus, their R, G, B values are all higher than 140. Simultaneously, they are greyer and not colourful compared to other parts of the highway, such as green or brown side slopes and vegetation; thus, the absolute values of the differential values between their R, G, B values are lower than 50.

Alternatively, the colours of road markings are quite different from surrounding pavement point clouds, so their (R+G+B) values have significant differential values compared to the average (R+G+B) values of the surrounding point clouds. Besides, side slope point clouds can be greener than pavement point clouds; thus, their G values are significantly higher than R and B values.

Similarly, road verge point clouds can be yellower than pavement point clouds; thus, their B values are significantly lower than R and G values. The coloured pavement point clouds are divided into different sections. Since in different sections, the corresponding aerial photograph has different colour tones, sunlight impacts, and vegetation impacts, the parameters (e.g." higher than 140", "lower than 50" mentioned above) for point clouds extraction in the algorithm should be set and adjusted according to actual circumstances to realise ideal target point clouds abstraction. Target point clouds representing different pavement parts with different features can be obtained.

3.2 Horizontal alignment fitting

This section provides a novel workflow for horizontal alignment fitting from map data. The alignment fitting is mainly based on the road marking line point clouds. Unlike the controllable field survey, aerial photographs are obtained by satellite orthographic photography. The aerial photographs have different hues, and the road marking can be affected by shadows, trees and other objects. Besides, due to wear and tear, the road markings are missing in some sections, and the sections with missing road markings are random and asymmetrical on the right side and the left side. The proposed approach can fit the alignment and get the alignment parameters considering these problems, as shown in Fig. 3.

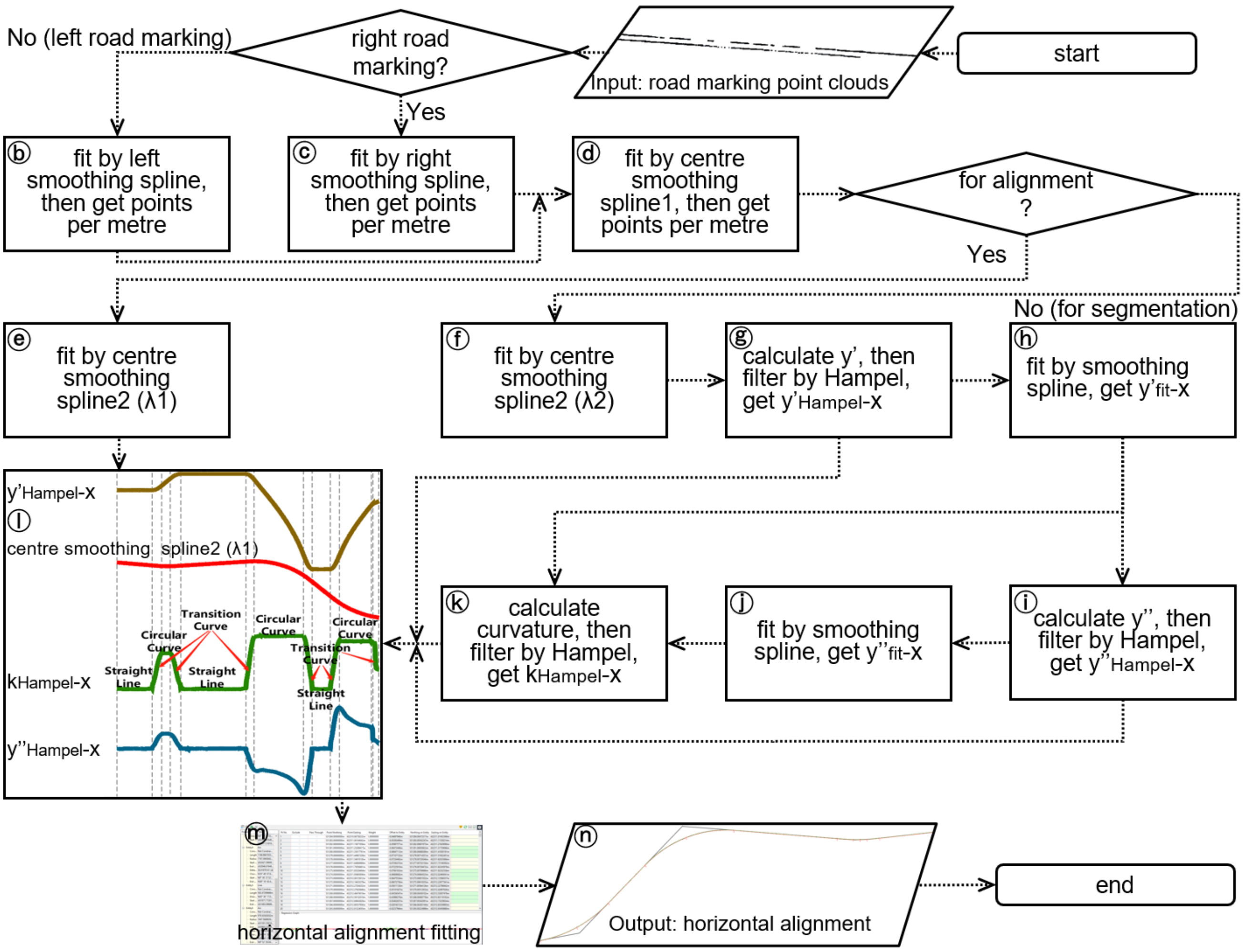

Fig. 3. The workflow of horizontal alignment fitting

After data acquisition and processing, point clouds of two road markings near the central reserve can be obtained. The point clouds data is noisy, and a smoothing spline can fit it. Smoothing splines are employed to fit road markings, and horizontal alignment, described by Equation (1), where f is any twice-differentiable function on [a,b] which is the function of the smoothing spline, and λ is the smoothing parameter. The smoothing spline aims to minimise $S(f)$. The parameter λ is defined between 0 and 1. $\lambda = 0$ produces a least-squares straight-line fit to the data, while $\lambda = 1$ produces a cubic spline interpolant that goes through all the data points [31]. Along the road, in some areas, road markings can be sheltered by an overpass or missing. Moreover, in some areas, tops of vehicles have similar colours compared to road markings; thus, some vehicles' point clouds can be extracted and mixed with road marking point clouds. Smoothing splines are quite flexible controlled by λ, and they always consider the balance of trying to go through all the point cloud clusters and considering the overall trends of the point. Thus, the local loss of point clouds cannot influence the overall trend of a smoothing spline. However, local mistakes such as deviations caused by other point clouds (e.g. car point clouds) can influence a smoothing spline's local shape. Thus, before fitting the road markings, all of the point clouds' local mistakes should be removed (fewer is better than wrong). After getting the point clouds of the two road markings near the central reserve, the centre horizontal alignment should not be fitted directly by the point clouds of two road markings together because, in some areas, some local point clouds on the one side are missing, while the local point clouds exist on the other side as shown in ⓐ in Fig. 3. It can cause significant local deviations of the centre line. Thus, based on our proposed approach, the two road markings near the central reserve are fitted separately by two smoothing splines called the left smoothing splines and the proper smoothing spline, respectively, as shown in ⓑ and ⓒ in Fig. 3. After getting the two smoothing splines' functions, the points on the smoothing splines per metre along the x-axis can be obtained. Afterwards, the centre line can be fitted by a smoothing spline called centre smoothing spline one according to the points per metre on the left and proper smoothing splines as shown in ⓓ in Fig. 3.

Similarly, the points on the centre smoothing spline 1 per metre along the x-axis can be obtained and based on which another smoothing spline called the centre smoothing spline two can be fitted to represent the centre horizontal alignment. According to the actual road marking point clouds, different λ values should be tested several times to choose an appropriate λ value for smoothing splines to ensure that the smoothing splines' deviations from road marking point clouds are not significant and smoothing splines do not fluctuate significantly. The RMSE value, calculated by Equation (2), can evaluate the deviation. Based on the function $f(x)$ of the centre smoothing spline 2, $f(x)$ values per metres along the x-axis are represented by y_{fit}. Two λ values can be selected for centre smoothing spline 2. The λ1 is for horizontal alignment fitting, and the λ2 is for horizontal alignment segmentation and parameter extraction, as shown in ⓔ and ⓕ in Fig. 3. The λ2 is much smaller than λ1, and the λ1 and λ2 will be introduced in the next paragraph.

$$S(f) = \lambda \sum_{i=1}^{n}((y_i - f(x_i))^2 + (1-\lambda)\int_a^b (f''(x))^2 dx \quad (1)$$

$$RMSE = \sqrt{\frac{1}{m}\sum_{i=1}^{m}(y_i - \widehat{y_i})^2} \quad (2)$$

After getting the centre smoothing spline 2 using λ2, the first derivatives on the spline per metre along the x-axis can be calculated and drawn into an image. Due to the smoothing splines' local fluctuation, some outliers and spikes are on the first derivative image. A filter method called the Hampel filter is employed to address this problem. The Hampel filter is a type of decision filters that replaces the central value in the data window with the median if it lies far enough from the median to be deemed an outlier. This filter depends on the window width and an additional tuning parameter t, reducing the median filter when t=0, so it may be regarded as another median filter extension. The filter method can be described by Equation (3)-(6), where W_i^n is moving data window, m_k is the median value from the moving data window and S_k is the MAD scale estimate. The factor 1.4826 makes the MAD scale estimate an unbiased estimate of the standard deviation for Gaussian data [33]. All the first derivatives of the centre smoothing spline two using λ2 are regarded as x_i in the Equation (3)-(6). After filtering the first derivatives using the Hampel filter, the filtered first derivatives are represented by y'_{Hampel} as shown in ⓖ in Fig. 3 and a smoothing spline can fit y'_{Hampel} values and their corresponding x, which is called the first derivative smoothing spline (y'_{fit}-x), as shown in ⓗ in Fig. 3. Similarly, first derivatives on the first derivative smoothing spline per metre along the x-axis can be calculated. Hampel filter is again employed to filter the first derivatives (second derivatives of the centre smoothing spline 2), and the results can be represented by y''_{Hampel} as shown in ⓘ in Fig. 3. A smoothing spline is employed to fit y''_{Hampel} values with their corresponding x values which is called the second derivative smoothing spline (y''_{fit}-x), as shown in ⓙ in Fig. 3. Each y values per metre along the x-axis on the first derivative smoothing spline and on the the second derivative smoothing spline can be regarded as the first derivative y'_{fit} and the second derivative y''_{fit} of the centre smoothing spline 2 using λ1 or λ2. The curvature values k of the horizontal alignment can be calculated by Equation (7), and their reciprocals are the radius of curvature r. Afterwards, the curvature values can also be filtered by Hampel filter to obtained filtered curvature values k_{Hampel} which can be regarded as curvature values of the horizontal alignment, as shown in ⓚ in Fig. 3. Four images can be drawn in CAD by writing and loading scr scripts, namely, the centre smoothing spline 2 using λ1 (y_{fit}- x image), y'_{Hampel} -x image, y''_{Hampel}-x image and k_{Hampel}-x image. The y_{fit}- x (using λ1) image is employed to fit the final horizontal alignment, while the y'_{Hampel} -x, y''_{Hampel}-x , k_{Hampel}-x images are emplpoyed to determine parameters and segmentations of different elements of the centre smoothing spline 2 using λ1 instead of using fitted values such as y'_{fit} and y''_{fit} because their edges and corners are more obvious. Due to the fluctuation of the smoothing splines, in this paper, two λ values can be employed to fit the centre smoothing spline 2, as mentioned above. λ1 is employed to determine y_{fit}- x image with a relatively high precision, however its y'_{Hampel} -x image, y''_{Hampel}-x , k_{Hampel}-x images have many noises and bad shapes. λ2 is much smaller than λ_1 which is employed to determine y'_{Hampel} -x, y''_{Hampel}-x , k_{Hampel}-x. Though its y_{fit}- x have relatively apparent deviations from the point clouds at the start point and the endpoint, its y_{fit}- x is much smoother, and its y'_{Hampel} -x, y''_{Hampel}-x , k_{Hampel}-x images have fewer noises and good shapes. Though there are deviations between the two y_{fit}- x images using λ_1 and λ_2, it is accurate enough to implement y'_{Hampel} -x image, y''_{Hampel}-x , k_{Hampel}-x images using λ_2 instead of λ_1 to determine the parameters and segmentations of different elements. The four images can be drawn in CAD with appropriate scales, as shown in ① in Fig. 3.

$$W_i^n = \{x_{i-n}, \dots, x_i, \dots, x_{i+n}\} \tag{3}$$

$$m_i = median\{x_{i-n}, \dots, x_i, \dots, x_{k+n}\} \tag{4}$$

$$y_i = \begin{cases} x_i & |x_i - m_i| \le tS_i \\ m_i & |x_i - m_i| > tS_i \end{cases} \tag{5}$$

$$S_i = 1.4826 \times median_{j\in[-n,n]}\{|x_{i-j} \; - \; m_i \;|\} \tag{6}$$

$$\frac{1}{r} = k = \frac{\left|y''_{fit}\right|}{(1+y'^2_{fit})^{\frac{3}{2}}} \tag{7}$$

In road engineering, a horizontal alignment can be described by straight lines, circular curves, and transition curves. Transition curves are clothoid. Straight lines and circular curves can be briefly described by Equation (8) and Equation (9). The polar coordinate equation of a clothoid is shown in Equation (10). All the clothoid curves can be regarded as a section of an entire clothoid curve starting from (0,0) with the original direction of (1,0) vector and zero curvature. l_s denotes the mileage (cumulative length) on the entire transition curve of a specific point from (0,0), and R denotes the curvature radius at the specific point. l and r respectively denote the mileage and the curvature radius of any point on the entire transition curve from (0,0). A denotes the parameter of the clothoid. The Cartesian coordinate equation of any point on the transition curve can be obtained through Equation (11) - (12). For straight-line sections, in the y'_{Hampel} -x image; the image is parallel to x-axis. In the y''_{Hampel}-x image, y''_{Hampel} is zero, and the image goes along the x-axis. In the k_{Hampel}-x image, k_{Hampel} is zero, and the image goes along the x-axis. For circular curve sections, in the k_{Hampel}-x image, k_{Hampel} is a certain value representing its curvature, and the image is parallel to x-axis. The other segmentations in the k_{Hampel}-x image with other shapes represents transition curves. The centre smoothing spline 2 using λ1 can be divided into straight-line sections, circular curve sections and transition curve sections. Based on different sections, straight lines, circular curves, and transition curves can be fitted by Civil 3D directly or by Equation (8), (9), (11), (12) using the least square method, and then based on the different elements, a horizontal alignment can be established in civil 3D.

$$y = ax + b \tag{8}$$

$$(x-a)^2 + (x-b)^2 = R^2 \tag{9}$$

$$l_s R = lr = A^2 = \frac{1}{a^2} \tag{10}$$

$$x = \sum_{n=0}^{+\infty} \frac{(-1)^n a^{2n} l^{4n+1}}{(2n)!(4n+1)2^{2n}} = l - \frac{l^5}{40R^2 l_s^2} + \frac{l^9}{3456R^4 l_s^4} - \cdots \tag{11}$$

$$y = \sum_{n=0}^{+\infty} \frac{(-1)^n a^{2n+1} l^{4n+3}}{(2n+1)!(4n+3)2^{2n+1}} = \frac{l^3}{6Rl_s} - \frac{l^7}{336R^3 l_s^3} + \cdots \tag{12}$$

3.3 Vertical alignment fitting

This section's proposed method can fit the vertical alignment and obtain the parameters from the map data. It also can reduce the influence of outliers and spikes of elevations caused by pavement defects and overpasses, as shown in Fig. 4. Also, vehicle point clouds can also cause outliers and spikes of elevations. Though they cannot influence the vertical alignment fitting, they can influence the cross-section's elevation, which will be introduced in Section 3.4. The overall workflow can be shown in Fig. 5.

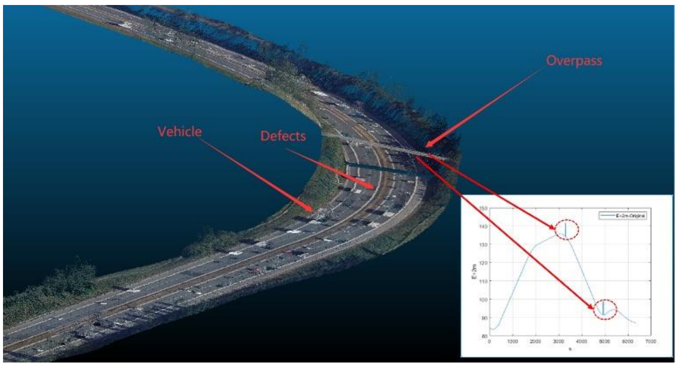

Fig. 4. Causes of point clouds' outliers and spikes

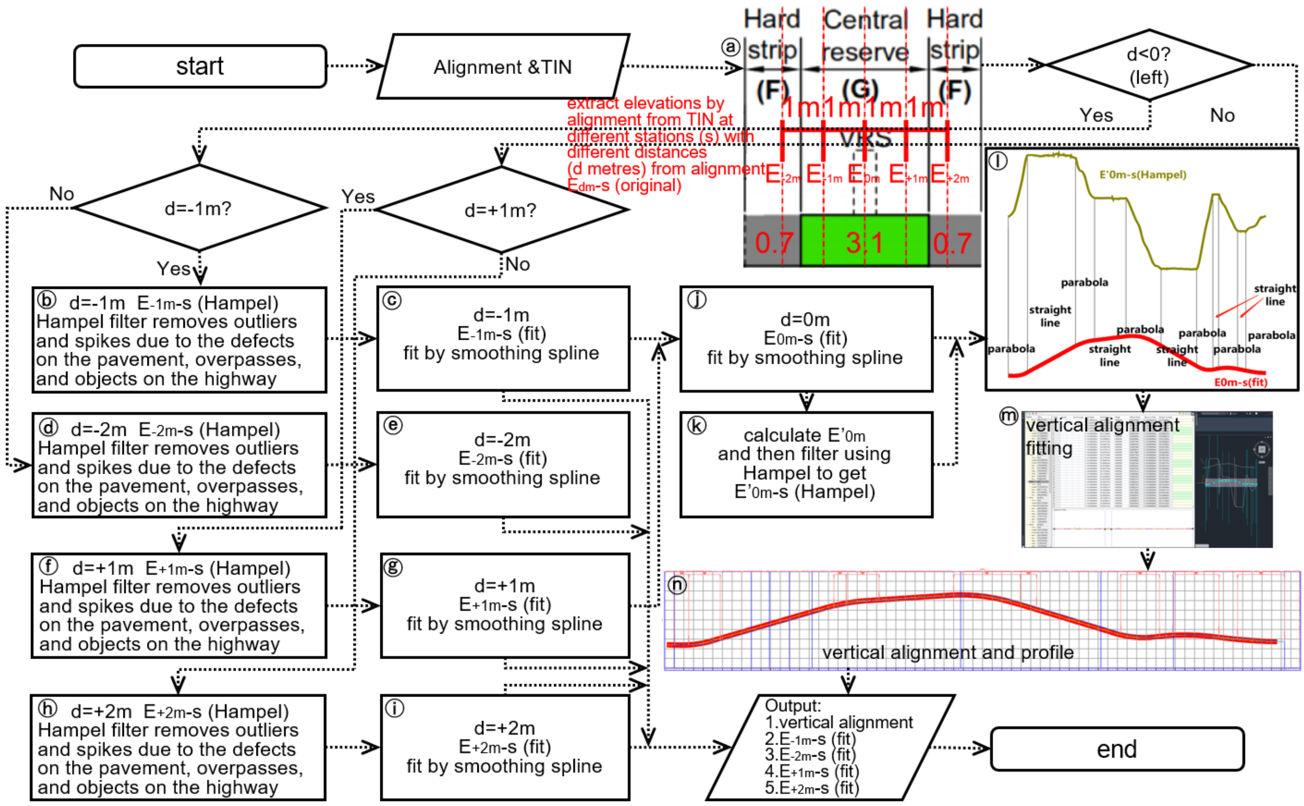

Fig. 5. The workflow of vertical alignment fitting

After establishing the horizontal alignment, the alignment station can be determined (e.g., the start point station is K0+000.000, and the endpoint's station is K7+000.000). The elevations along the horizontal alignment can be extracted from the TIN model of point clouds, including highway and surrounding areas. There are guardrails installed along with the centre reverse for some existing old highway, which can influence the elevation. Also, due to defects caused by wear and tear, the centre reverse is uneven, and its edge between the pavement is blurry. Thus, offset horizontal alignments and extract the elevations of them to control the elevation of the highway digital twin. For example, the elevations of positions on the TIN with 1m and 2m horizontal distance on the left and right sides from the horizontal alignment can be extracted, as shown in ⓐ in Fig. 5. The elevations can have many outliers and spikes, as shown in Fig. 4; thus, Hampel filter with appropriate n and t values as mentioned in Equation (3)-(6) is implemented to remove them, as shown in ⓑ, ⓓ, ⓕ, ⓗ in Fig. 5. Afterwards, smoothing splines with appropriate λ, as mentioned in Equation (1) values are employed to fit the elevations with their corresponding stations, as shown in ⓒ, ⓔ, ⓖ, ⓘ in Fig. 5. Then, each elevation E_{dm} on the smoothing spline (d denotes the horizontal distance from the alignment. "-" refers to on the left side and "+" refers to on the right side. m refers to the metre) per metre of stations (s) can be computed using the smoothing spline. E_{0m} can be inferred by the equation $E_{0m} = (E_{-1m} + E_{+1m})/2$. Then a smoothing spline is employed to fit E_{0m} and stations (s) to obtain E_{0m}-s image, as shown in ⓙ in Fig. 5. Next, the first derivative of the smoothing spline can be calculated. Similarly, the Hampel filter is employed to filter the first derivative values and the filtered first derivative E'_{0m} per metre of stations can be obtained, as shown in ⓚ in Fig. 5. Thus, the E_{0m}-s image and E'_{0m}-s can be drawn in CAD by programming, as shown in ⓛ in Fig. 5.

In road engineering, a vertical alignment can be described by straight lines and parabolas, as shown in Equation (13) and Equation (14). In straight-line sections of the E'_{0m}-s image, the image is parallel to s-axis. In the parabola sections of the E'_{0m}-s image, the image is a straight line. Thus, the smoothing splines of vertical alignment can be divided into straight-line sections and parabola sections. Based on different sections, straight lines can be fitted by Civil 3D directly or by Equation (13), (14) using the least square method, and then based on the different elements, a vertical alignment can be established in civil 3D. The vertical alignment, $E_{-2m} - s$, $E_{-1m} - s$, $E_{+1m} - s$, $E_{+2m} - s$ are employed to control the central elevation of the digital twin, which will be introduced in Section 3.4.

$$E_{dm} = as + b \tag{13}$$

$$E_{dm} = \frac{1}{2R}s^2 + bs + c \tag{14}$$

3.4 Cross-section processing

Since the original map data's quality is relatively poor, the TIN of the highway's surface fluctuates significantly and has may outliers. This section gives a novel workflow to determine different components, including central reserves, hard strips, lanes, shoulders, verges, and side slopes, using the map data to assist in digital twinning. Also, due to the long-term erosion, the boundary between the verge, the side slope and the position of the side slope' toe have become ambiguous. Besides, the side slope has changed. This section proposed a novel method to determine them for the highway digital twin. There are seven steps for cross-section processing, as shown in Fig. 6.

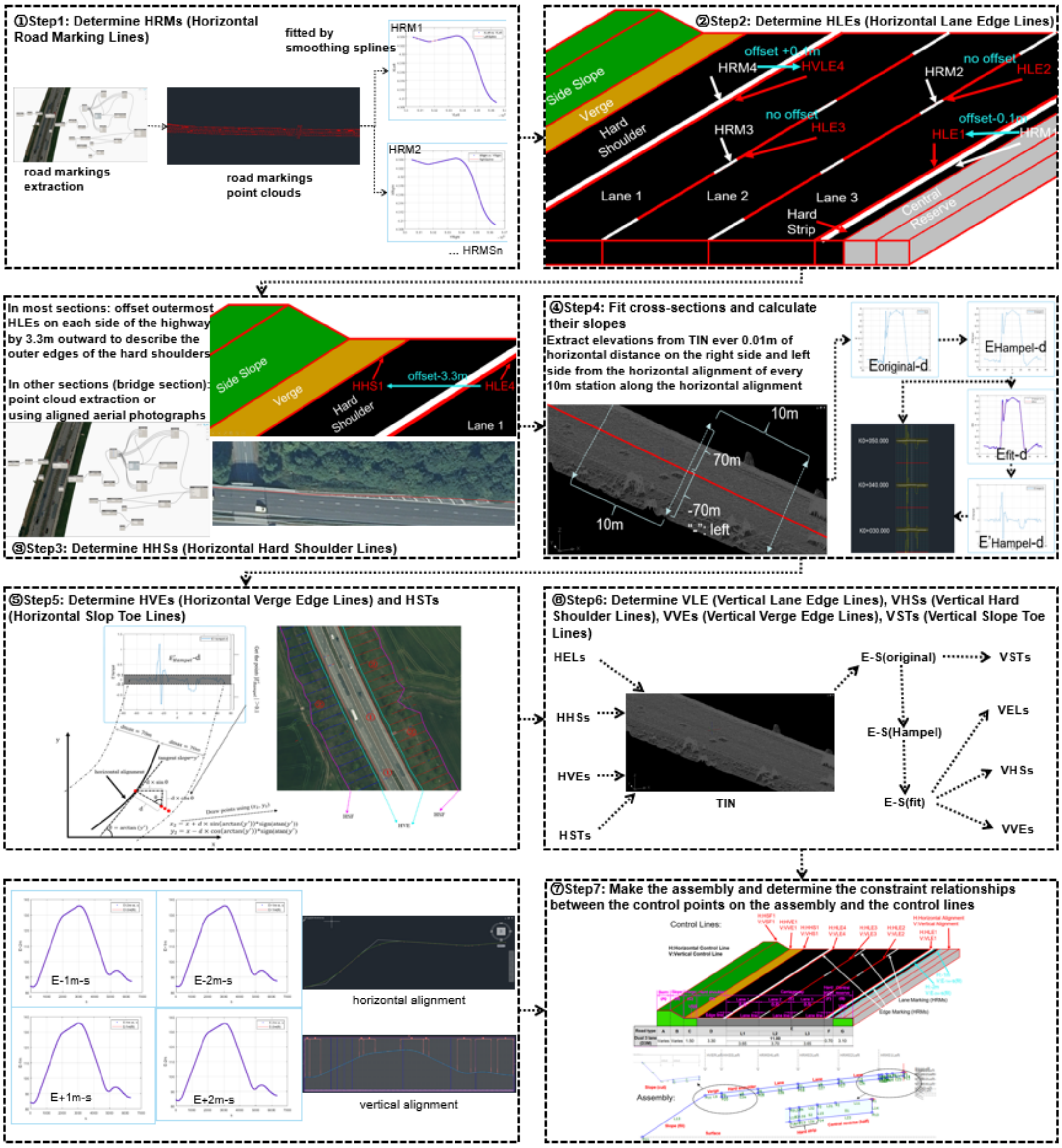

Fig. 6. The workflow of cross-section processing

First, determine HRMs (Horizontal Road Marking Lines), as shown in ① in Fig. 6. As is mentioned in Section 3.1 and Section 3.2, road marking point clouds can be selected from coloured pavement point clouds according to colours. Thus, all the road markings can be extracted, including edge markings that mark edges of carriageways using complete lines and lane markings that divide a carriageway into lanes using broken lines. Then smoothing splines are employed to fit the road markings' horizontal position, which is called HRMs. Also, the proper smoothing spline and the left smoothing are HRMs.

Second, determine HLEs (Horizontal Lane Edge Lines), as shown in ② in Fig. 6. The polylines that describe horizontal positions of edges of the lanes, including the edges of the carriageways, are called HLEs. According to UK Design Manual for Roads and Bridges [12], there may be some deviations between HLEs and HRMs. Generally, there is a 0.1m deviation between the edge of the carriageway and the edge marking such as HRM1, HRM4, HLE1, HLE4, while there is no deviation between other lane edges and their corresponding lane markings such as HRM2, HRM3, HLE2, HLE3. HRMs are offset or not offset according to the deviations to obtain polylines to describe the horizontal edges of the lanes (HLEs).

Third, determine HHSs (Horizontal Hard Shoulder Lines), as shown in ③ in Fig. 6. The polylines that describe horizontal positions of the outer edges of the shoulders are called HHSs. In most highway sections, the distance between the outermost HLE and the HHS is 3.3m based on the UK design manual [12]. In some positions, the distance is not 3.3m, such as the bridge sections. First, the outermost HLEs on each side of the highway can be offset by 3.3m outwards to describe the shoulders' outer edges. Then, modify the offset HLEs in some sections where the distance is not 3.3m. In these sections, the coloured pavement point clouds can be employed to extract the hard shoulder's outer edge by the approach proposed in Section 3.1. In addition to point cloud extraction, the aerial photographs can be aligned to the right position of the highway with the right scales in CAD to be employed to outline the outer edge of the hard shoulder.

Fourth, fit cross-sections and calculate their slopes, as shown in ④ in Fig. 6. After establishing the alignment, elevations on the TIN ever 0.01m of horizontal distance on the right side and left side from the horizontal alignment of every 10m station on the horizontal alignment can be extracted. The required maximum distance depends on the highway land use scope. In this research, the maximum distance is 70m on each side. A n*3 array can compile the elevation data, and each row can be described as (s,d, E) where s, d, E denote the station of the alignment, the horizontal distance from the alignment, and the elevation on the TIN, respectively. For cross-sections, there may be some outliers and spikes on the elevation data due to the point clouds of vehicles, defects, and some wrong point clouds due to the poor quality of the downloaded map data, as shown in Fig. 4. Thus, the Hampel filter is again employed to remove the outliers and spikes to obtain a new array, and each row can be described as (s,d, E_{Hampel}). Afterward, smoothing splines are employed to fit E_{Hampel}-d data for each cross-section per 10m of the stations. Then, the first derivative values can be calculated, and the Hampel filter is again employed to remove the outliers and spikes to obtain E'_{Hampel} data. A new array called Cross-section Array can be established and each row can be described as (s, d, E_{Hampel}, E'_{Hampel}). E'_{Hampel}-d can express slopes of the E_{Hampel}-d which can describe the values of the crossfalls and side slopes, including cut and fill slopes. Each point of the cross-section has the corresponding coordinate (s, d, E_{Hampel}, E'_{Hampel}) in the Cross-section Array.

Fifth, determine HVEs (Horizontal Verge Edge Lines) and HSTs (Horizontal Slop Toe Lines), as shown in ⑤ in Fig. 6. The polylines that express the verge's outer edge are called HVEs, and the polylines that express the edge of the slope toe are called HSTs. Due to the long-term erosion and the vegetation's growth, in some sections, the edges between verges and slopes are blurred, the slop toes are not distinct, and the side slopes have changed. In addition, due to the vegetation and similar construction materials of the verges and slopes (including cut and fill sections), it is hard to distinguish the edges between them. Thus, a feasible method is proposed. According to the UK design manual, for ordinary sections of the highway, the cross fall is usually 2.5%. However, in some sections, appropriate superelevation should be set, and usually, the maximum superelevation is 7%. Generally, the gradient of the side slope is no less than 1:3 [11,14]. Considering the maximum superelevation and the minimum gradient of the side slope, 0.1 (10% or 1:10) of E'_{Hampel} is used to distinguish the slope from the other parts of the road. For each point on the cross-section per 10m of the stations along the alignment, if its E'_{Hampel} is greater than 0.1 or less than -0.1, the point will be selected. Simultaneously, the station (s) and the horizontal distance to the alignment (d) of the point can be obtained by the (s, d, E_{Hampel}, E'_{Hampel}) coordinates from the Cross-section Array. After obtaining the horizontal alignment, for each corresponding station of the cross-section, the coordinates of the point on the horizontal alignment and the slope of the tangent lines at the point on the horizontal alignment can be calculated and expressed by (x,y) and y', respectively. The horizontal coordinate (x_2,y_2) of the selected points on the cross-section can be calculated by Equation (15)- (16), where $sign(\arctan(y'))$ denotes the sign of $\arctan(y')$. Afterwards, the selected points on all the cross-section can be drawn in the CAD in red or blue together with an aligned aerial photograph. The E'_{Hampel} of the red points are greater than 0.1 and the E'_{Hampel} of the blue is less than -0.1. At each station, a segmentation of continuous points with the same colour (red or blue) can be selected. Continuous segmentations of the points denote the side slop lines. Continuous pieces of the red points on the highway's left side and blue points on the highway's right side express the fill slopes. Conversely, continuous pieces of the blue points on the highway's left side and red points on the highway's right side express the cut slopes. If a piece of points intrudes on the pavement, it should be ignored, as shown by ① in Fig. 7. In addition, some defects on the continuous segmentation of the points with the same colour should also be ignored, such as a tiny piece of missing or a tiny piece of points with the other colour as shown by ② skip in Fig. 7. However, sometimes, a piece of missing points denote the berm between two slopes. Horizontal polylines link the inner ends of the continuous pieces of the points near the highway to obtain HVEs. The outer ends of the continuous piece s of the points near the highway are linked by horizontal polylines to obtain HSTs, as shown in Fig. 7. The aligned aerial photographs can also assist in determining the HVEs and HSTs, especially in bridge and culvert sections where the slope lines are very short or there are no slope lines.

$$x_2 = x + d \times \sin(\arctan(y')) \times sign(\arctan(y')) \quad (15)$$

$$y_2 = y - d \times \cos(\arctan(y')) \times sign(\arctan(y')) \quad (16)$$

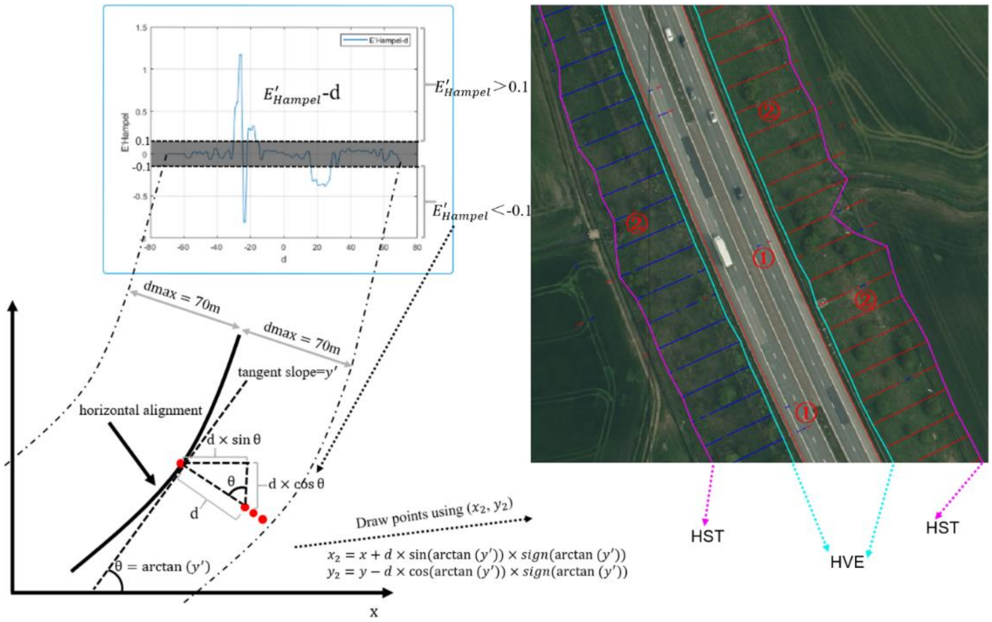

Fig. 7. The approach of determining the outer edge of a verge and the slope toe

Sixth, determine VLE (Vertical Lane Edge Lines), as shown in ⑥ in Fig. 6, VHSs (Vertical Hard Shoulder Lines), VVEs (Vertical Verge Edge Lines), VSTs (Vertical Slope Toe Lines). All the horizontal control lines (HLEs, HHSs, HVEs and HSTs) can be regarded as independent alignments with their own stations from the start point to the end point. All the horizontal control lines can extract elevations ($E_{original}$) from the TIN at each station (s) along the horizontal control lines. Thus, $E_{original}$-s data of horizontal control lines can be obtained. In order to achieve a smooth highway surface, $E_{Original}$-s of HLEs, HHSs, HVEs should be filtered by the Hampel filter and fitted by smoothing splines as expressed by Equation (1)-(6) to obtain E_{fit}-s. However, $E_{original}$-s of HSTs do not need to be filtered or fitted and can be used directly for modelling. Thus, the slope toes can match the terrain of the TIN. The E_{fit}-s of HLEs, HHSs, HVTs and $E_{original}$-s of HSTs are called VLEs, VHSsm VVEs and VSTs (vertical control lines), respectively.

Seventh, make the assembly of the road model according to the horizontal and vertical control lines and determine the constraint relationships between the control points on the assembly and the control lines, as shown in ⑦ in Fig. 6. An assembly of the highway is a 2D model that can express the cross-sections of the highway. The assembly has several control points that can be constrained to and go along the horizontal and vertical control lines to establish the highway digital twin model. When establishing an assembly of the highway, the left and right part of a cross-section employ the same method. Thus, only the left part of a cross-section is discussed. In this section, a three-lane highway assembly is taken as an example. The assembly and its corresponding control lines can be shown in Fig. 8, and their constraint relationships can be expressed in Table 1. Points in Table 1 are the corresponding points in Fig. 8. The offset constraints and the elevation constraints are controlled by corresponding control lines listed in Table 1, and some constraints are constants which mean the offset is 1m or 2m to the horizontal alignment on the left. The pavement thickness of the assembly can be set properly and approximately according to the design standard, which is not the focus of this article.

By using the proposed method, the wide variations of each component of the cross-section can be controlled by horizontal control lines flexibly. The elevations of the components of the cross-section can be controlled by vertical control lines flexibly. Thus, the road's cross fall and superelevation do not need to be calculated and can be expressed automatically.

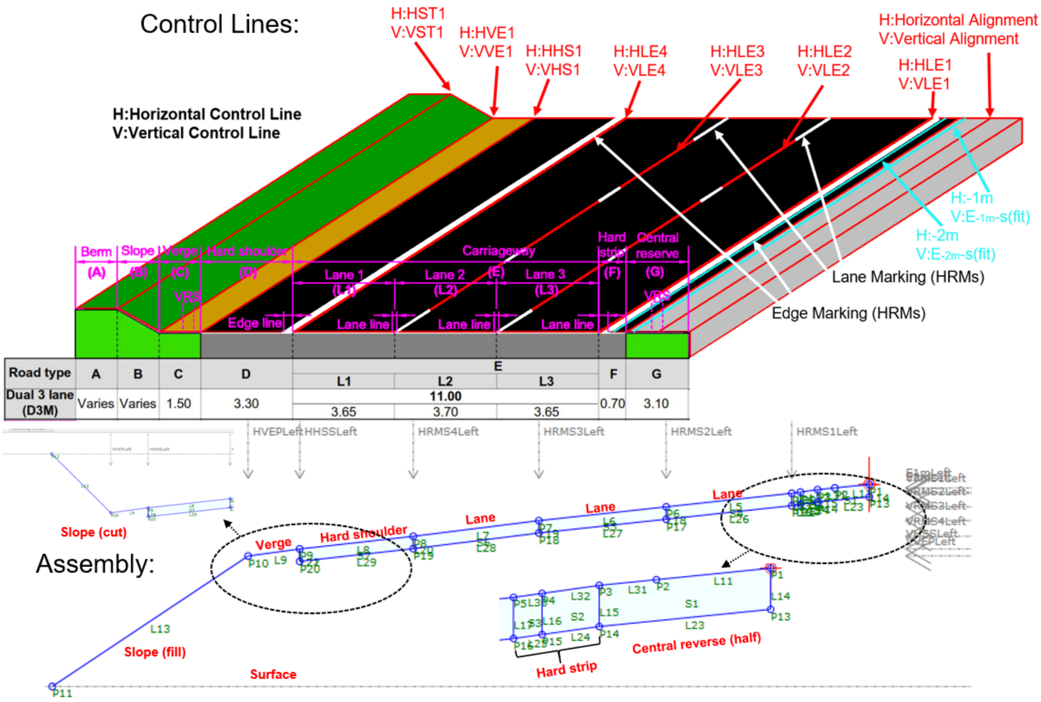

Fig. 8. The assembly and its corresponding control lines

Table 1. Control points on the assembly and their corresponding control lines

Point	Offset Constraint	Elevation Constraint	Point	Offset Constraint	Elevation Constraint
P1(Origin)	Horizontal alignment	Vertical alignment	P2	-1m	E_{-1m}-s (fit)
P4	-2m	E_{-2m}-s (fit)	P5	HLE1	VLE1
P6	HLE2	VLE2	P7	HLE3	VLE3
P8	HLE4	VLE4	P9	HHS1	VHS1
P10	HVE1	VVE1	P11	HST1	VST1

3.5 Digital twinning

Based on the processed data, alignment and cross-section processing, highway digital twin can be made using Civil 3D. In Civil 3D, horizontal alignment and its vertical alignment and profiles can be established. E_{dm}-s, HLESs, VLEs, HHSs, VHSs, HVEs, VVEs, HSTs and VSTs can be covert into 3D feature lines or 3D polylines to control the corresponding points of the assembly. Then, the assembly can go along the vertical and horizontal control lines, and the highway digital twin can be established. Since the existing old highway has been built, the original terrain has been modified and covered by the highway. However, the covered terrain under the highway is not essential for digital twinning. The HST on the right side and the HST on the right side can be combined to form a closed polyline that expresses the highway digital twin's outer contour. Afterwards, the closed polyline is employed to hollow the TIN. The aligned aerial photographs can attach the hollowed TIN. Finally, the highway digital twin model and the hollowed TIN attached with aligned aerial photographs can establish the overall digital twin.

4 CASE STUDY

Our proposed approach has been implemented to make a digital twin for a section of A1(M) motorway using downloaded data from Digmap. The data includes aerial photography, digital surface model (DSM) and topographies.

4.1 Project introduction

The A1 road is the longest numbered road in the UK which is 660 km and connects London with Edinburgh. The Ministry of Transport designated it in 1921, and for much of its route, it follows various branches of the historic Great North Road. Several sections of the route have been upgraded to motorway standard and designated A1(M). The scope of the case study section is between J60 Bradbury Interchange and J61 Bowburn Interchange. In this section, the A1 road has been upgraded to motorway standard and opened in 1969. This section is a two-way two-line motorway. In this research, the geographic coordinate of the start point of the digital twin section is 54°40'6.75"N 1°29'57.54"W and the geographic coordinate of the end point is 54°43'16.40"N 1°31'18.31"W as shown in Fig. 9.

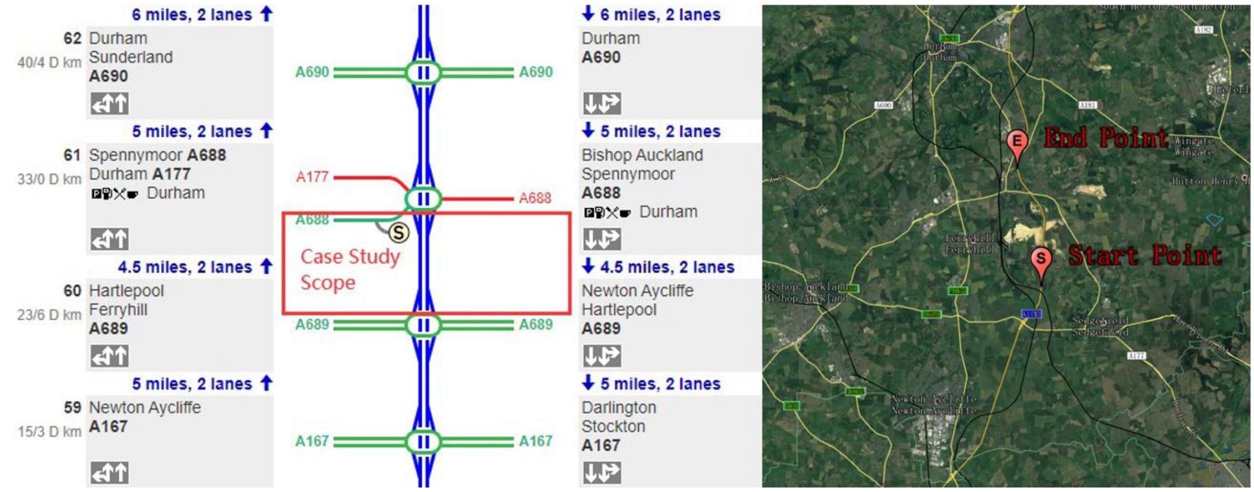

Fig. 9. The location of the highway in the case study

4.2 Horizontal alignment and evaluation

Base on the downloaded data from Digimap and the proposed method in Section 3, the horizontal alignment can be fitted. Since the A1 road is a major north-south road and for each y-coordinate, there is only one corresponding x-coordinate, y-coordinate (north-south) of the road map data is regarded as x-coordinate and x-coordinate (east-west) of the road map data is regarded as y-coordinate for fitting, filtering, derivatives, and curvature computing as mentioned in Section 3.2. The fitting, filtering and computing results and process of the alignment, first derivatives, second derivatives and curvatures can be shown in Fig. 10. The results of the left and right smoothing spline can be shown in Image ⓐ and ⓑ. Then, the centre smoothing spline 1 can be fitted (Image ⓒ). Image ⓓ and Image ⓔ show the results of centre smoothing spline 2 using λ1 and λ2, respectively. Smoothing spline 2 using λ1 (Image ⓓ) can be imported into Civil 3D after swapping the x-coordinates and y-coordinates (Image ⓕ). Based on Smoothing spline 2 using λ2 (Image ⓔ), y'_{Hampel}-x, y'_{fit}-x, y''_{Hampel}-x, y''_{fit}-x can be calculated and obtained, as shown in Image ⓗ, ⓖ, ⓚ, ⓙ respectively. According to y''_{fit}-x, k_{Hampel}-x can be calculated and obtained (Image ⓘ). Afterwards, y'_{Hampel}-x, y''_{Hampel}-x, k_{Hampel}-x can be imported into Civil 3D (Image ⓕ). Finally, smoothing spline 2 using λ1 can be divided into different segmentations to be fitted by straight lines, circular curves, and clothoid to obtain the final horizontal alignment (Image ⓕ). The detailed process was introduced in Section 3.2. The parameters and evaluation of each computing step in Fig. 10 can be shown in Table 2. Each row of Table 2 describes the corresponding image in Fig. 10. If the method is smoothing spline fitting, it will have parameters like λ, RMSE, and R-square, where λ and RMSE are introduced in Section 3.2. R-square denotes the coefficient of determination of the smoothing spline fitting. Through the change of data, R-square can characterise the quality of the fit. The normal value range of R-square is [0 1]. The closer it is to 1, the stronger the explanatory power of the equation's variables is for y, and the model fits the data better. If the method is Hampel filtering, there are no λ, RMSE, or R-square values, but the n, t parameters can be shown in Table 2, where n, t parameters are introduced in Section 3.2. The final horizontal alignment can be described in Table 3, where type denotes the type of an element of the alignment, such as a straight line, spiral (clothoid) and curve. The start station, end station, the coordinate of the start point and end point, the length of each element can be shown in Table 3. In addition, the radius denotes the radius of a curve element and A denotes the parameter of a spiral (clothoid) which was introduced in Equation (10). In the straight-line section, the alignment does not change the direction; however, in the curve and spiral section, the alignment changes its directions. Thus, the direction in Table 3 denotes the constant direction of a straight line, and the start direction and the end direction denotes the tangent directions at the start point and the end point of a curve or a spiral. The delta angle refers to the absolute value of the change in the direction at the start point and the end point of a curve or a spiral. The definition of a spiral is a clothoid, and the radius in and radius out denote the radius of curvature at the start point and the end point of a spiral.

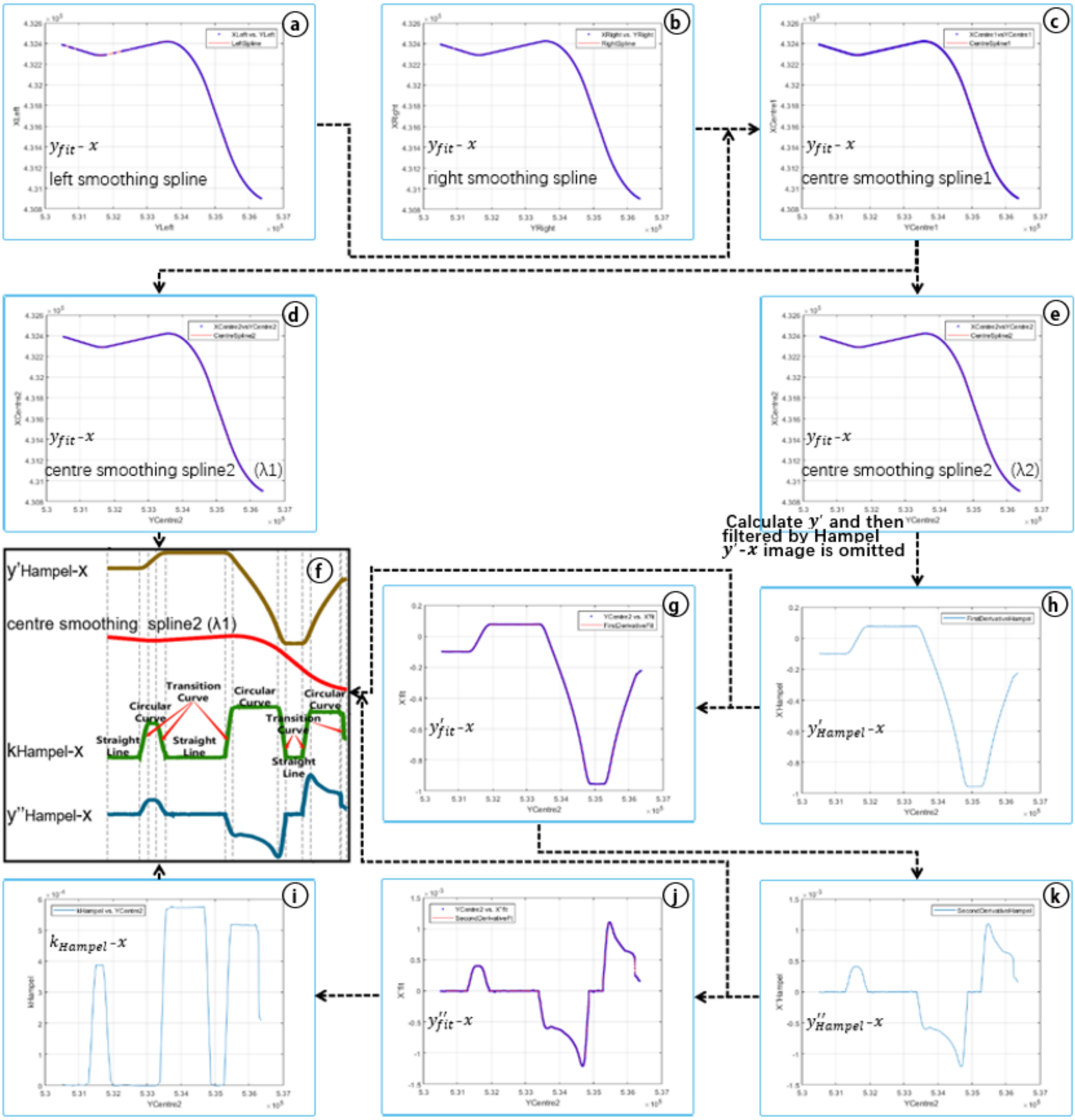

Fig. 10. The horizontal alignment fitting result

Table 2. Fitting parameters and evaluation of horizontal alignment

Name	Image in Fig. 10	Method	λ	RMSE	R-square	n	t
left smoothing spline	ⓐ	Smoothing spline fitting	1.670E-5	0.1593	1		
right smoothing spline	ⓑ	Smoothing spline fitting	1.670E-5	0.1662	1		
centre smoothing spline	ⓒ	Smoothing spline fitting	1.670E-5	2.51	1		
centre smoothing spline2 using λ1	ⓓ	Smoothing spline fitting	3.010E-3	0.004266	1		
centre smoothing spline2 using λ2	ⓔ	Smoothing spline fitting	1.371E-7	0.1825	1		

y'_{Hampel}-x	ⓗ	Hampel filtering				150	0.1
y'_{fit}-x	ⓖ	Smoothing spline fitting	0.01	6.006E-5	1		
y''_{Hampel}-x	ⓚ	Hampel filtering				30	0.1
y''_{fit}-x	ⓙ	Smoothing spline fitting	0.01	2.132E-6	1		
k_{Hampel}-x	ⓘ	Hampel filtering				200	0.1

Table 3. Horizontal alignment information

No.	Type	Start Station	End Station	Start Point(m) x= y=	End Point(m) x= y=	Length(m)	Radius(m)	A(m)
1	Line	K0+000.0000	K0+800.8946	432390.2367 530500.0062	432309.7170 531296.8429	800.8946		
2	Spiral	K0+800.8946	K0+987.1465	432309.7170 531296.8429	432293.4452 531482.3696	186.2519		661.1935
3	Curve	K0+987.1465	K1+194.8646	432293.4452 531482.3696	432289.6834 531690.0005	207.7181	2651.9031	
4	Spiral	K1+194.8646	K1+431.2892	432289.6834 531690.0005	432303.4164 531925.9933	236.4246		708.8826
5	Line	K1+431.2892	K2+972.6586	432303.4164 531925.9933	432417.5414 533463.1320	1541.3694		
6	Curve	K2+972.6586	K4+428.6781	432417.5414 533463.1320	431935.7054 534792.7823	1456.0195	1747.3939	
7	Line	K4+428.6781	K5+181.3551	431935.7054 534792.7823	431416.5728 535337.7814	752.677		
8	Curve	K5+181.3551	K6+334.8277	431416.5728 535337.7814	430903.3254 536351.9982	1153.4725	1947.5678	

No.	Direction	Delta Angle	Spiral Definition	Radius in	Radius out	Start Direction	End Direction
1	N5° 46' 12.3661"W						
2		2.2732(d)	Clothoid	infinitely great	2347.2350m	N5° 46' 12.3661"W	N3° 29' 48.8639"W
3		4.4879(d)				N3° 16' 54.7391"W	N1° 12' 21.5600"E
4		3.1866(d)	Clothoid	2125.4754m	infinitely great	N1° 12' 21.5600"E	N4° 23' 33.3617"E
5	N4° 14' 46.1066"E						
6		47.7418(d)				N3° 57' 05.4362"E	N43° 47' 25.1305"W
7	N43° 36' 27.1644"W						
8		33.9342(d)				N43° 48' 32.0889"W	N9° 52' 29.0570"W

4.3 Vertical alignment and evaluation

Based on the proposed method in Section 3.3, the overall process and results can be shown in Fig. 11. Image ⓐ, ⓓ, ⓗ, ⓛ are the original elevations on the DSM for each station at the position with the 1m and 2m distance to the horizontal alignment on both left and right sides, and they can be filtered (Image ⓑ, ⓔ, ⓘ, ⓜ) and fitted (Image ⓒ, ⓕ, ⓙ, ⓝ) by the Hampel method and smoothing splines. The central vertical alignment can be determined by using a smoothing spline to fit $(E_{-1m} + E_{+1m})/2$-s to form E_{0m}-s (Image ⓖ). Then the first derivative can be calculated and filtered by the Hampel method to form E'_{0m}-s image (Image ⓚ). E'_{0m}-s (Hampel) is employed to divided E_{0m}-s (fit) into different segmentations to make the central alignment be fitted by straight lines and parabolas separately (Image ⓞ). The parameters for each step can be shown in Table 4, where the corresponding names and their corresponding images in Fig. 11 can be shown in the first and second columns. Similarly, If the method is smoothing spline fitting, it will have parameters like λ, RMSE, and R-square. If the method is Hampel filtering, it will have parameters like n and t. λ, RMSE, n and t were introduced in Section 3.2, and R-square was introduced in Section 4.2. The final central vertical alignment can be expressed in Table 5. PVI denotes the point of vertical intersection where the vertical slope changes. Grade in and grade out denote the slope in front of the PVI and the slope behind the PVI, respectively. If the sub-entity type of a PVI is symmetric parabola, it means that the PVI is at the middle of a curve, such as the rows of No.2, No.4, No.7, No.9, No. 12, No.14, No. 17, No.20, and No.23. The sag and crest mean a sag curve and a crest curve, respectively. If there is only one PVI with a blank content at the sub-entity type column, it means that the PVI is just between two connected parabolas, such as the rows of No.3, No.8, and No.13. If there are two adjacent PVIs with a blank content at the sub-entity type column, it means that PVIs are the start point and the end point of a straight line between two parabolas, such as the rows of No.5, No.6, No.10, No.11, No.15, No.16, No.18, No.19, No.21, and No.22. The rows of No.1 and No. 24 are the start point and the end point of the verticle alignment. Profile curve length, K value, curve radius are the typical parameters of a parabola of vertical alignment in road engineering.

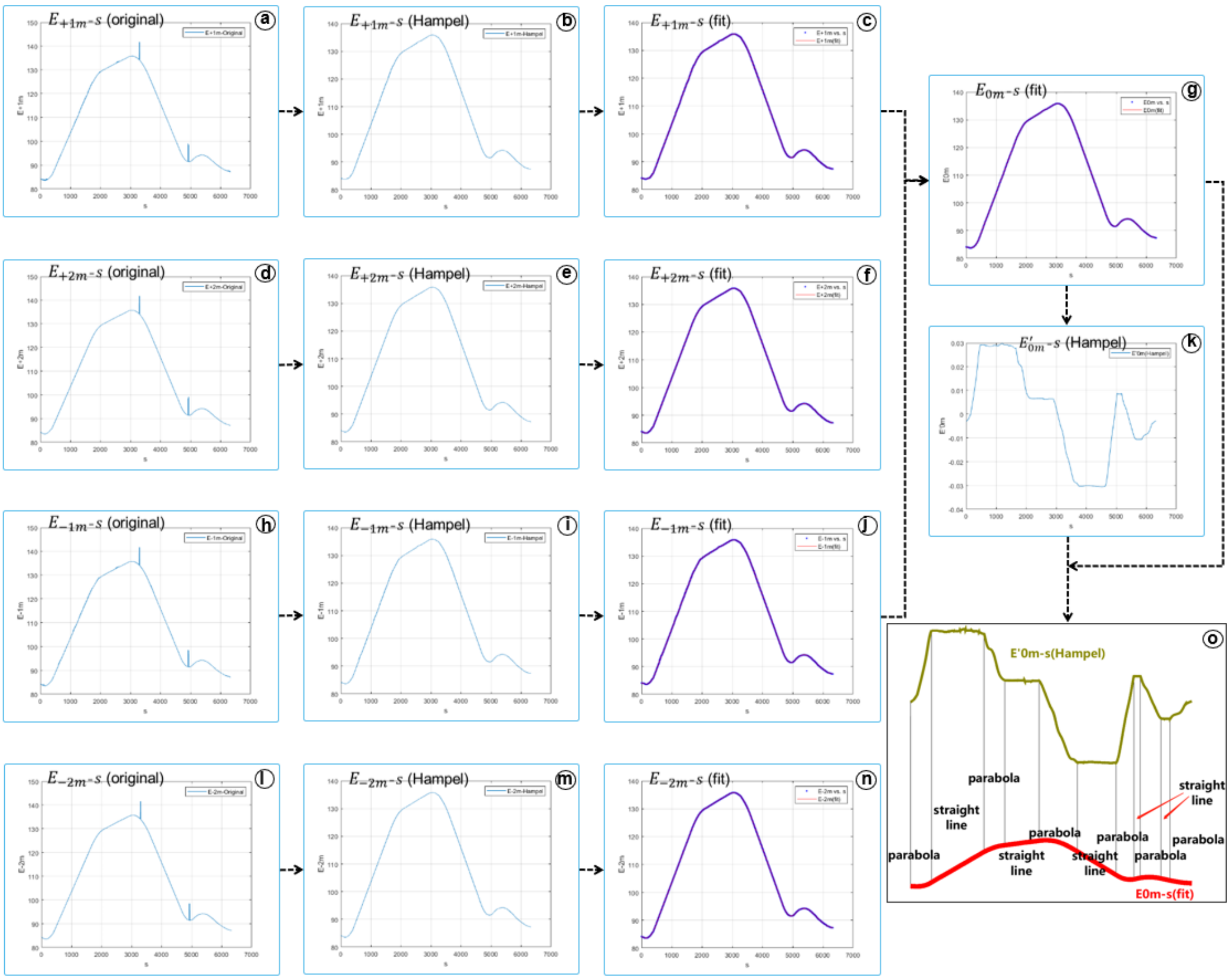

Fig. 11. The vertical alignment fitting result

Table 4. Fitting parameters and evaluation of vertical alignment

Name	Image in Fig. 11	Method	λ	RMSE	R-square	n	t
E_{-1m}-s (Hampel)	ⓑ	Hampel filtering				60	0.1
E_{-1m}-s (fit)	ⓒ	Smoothing spline fitting	1.6698E-6	0.03995	1		
E_{-2m}-s (Hampel)	ⓔ	Hampel filtering				60	0.1
E_{-2m}-s (fit)	ⓕ	Smoothing spline fitting	1.6698E-6	0.02558	1		

E_{+1m}-s (Hampel)	ⓘ	Hampel filtering				60	0.1
E_{+1m}-s (fit)	ⓙ	Smoothing spline fittting	1.6698E-6	0.04463	1		
E_{+2m}-s (Hampel)	ⓜ	Hampel filtering				60	0.1
E_{+2m}-s (fit)	ⓝ	Smoothing spline fitting	1.6698E-6	0.02752	1		
E_{0m}-s (fit)	ⓖ	Smoothing spline fitting	1.6698E-6	0.008	1		
E'_{0m}-s(Hampel)	ⓚ	Hampel filtering				150	0.1

Table 5. Vertical alignment information

No.	PVI Station	PVI Elevation(m)	Grade in	Grade out	Profile Curve Type	Sub-entity Type	Profile Curve Length(m)	K Value	Curve Radius(m)
1	K0+005.0	84.1679		-0.40%					
2	K0+077.5	83.8785	-0.40%	-0.08%	Sag	Symmetric Parabola	145.000	459.993	45999.313
3	K0+150.0	83.8176	-0.08%	-0.16%					
4	K0+314.0	83.5545	-0.16%	2.98%	Sag	Symmetric Parabola	328.000	104.522	10452.241
5	K0+478.0	88.4378	2.98%	2.90%					
6	K1+657.0	122.6302	2.90%	2.76%					
7	K1+720.5	124.3849	2.76%	1.92%	Crest	Symmetric Parabola	127.000	149.800	14980.041
8	K1+784.0	125.6013	1.92%	2.27%					
9	K1+955.5	129.4868	2.27%	0.39%	Crest	Symmetric Parabola	343.000	182.985	18298.511
10	K2+127.0	130.1576	0.39%	0.66%					
11	K2+900.0	135.2257	0.66%	0.81%					
12	K3+246.0	138.0364	0.81%	-2.89%	Crest	Symmetric Parabola	692.000	186.810	18681.029
13	K3+592.0	128.0302	-2.89%	-2.78%					
14	K3+677.0	125.6674	-2.78%	-3.02%	Crest	Symmetric Parabola	170.000	693.208	69320.769
15	K3+762.0	123.0962	-3.02%	-3.02%					
16	K4+634.0	96.7273	-3.02%	-3.27%					
17	K4+835.0	90.1484	-3.27%	0.88%	Sag	Symmetric Parabola	402.000	96.863	9686.293
18	K5+036.0	91.9115	0.88%	1.09%					
19	K5+176.0	93.4407	1.09%	0.83%					
20	K5+415.5	95.4216	0.83%	-1.14%	Crest	Symmetric Parabola	479.000	243.202	24320.250
21	K5+655.0	92.6854	-1.14%	-1.09%					
22	K5+847.0	90.5988	-1.09%	-1.12%					
23	K6+091.0	87.8558	-1.12%	-0.18%	Sag	Symmetric Parabola	488.000	519.548	51954.825
24	K6+335.0	87.4046	-0.18%						

4.4 Cross-section, digital twin and evaluation

Base on the proposed method in Section 3.4, the road marking point clouds can be extracted from the coloured pavement point clouds to obtain HRMs. Based on the UK Traffic Signs Manual, the edge of carriageway road markings (edge markings) are 200mm wide full lines, and road markings that divide a carriageway into lanes (lane markings) are 150mm wide broken lines [42]. The size can be shown in Fig. 13. As shown in Fig. 8, there is no deviation between a lane marking and an HLEs. However, there is a 0.1m deviation between an edge marking and an HLE. The HLEs can be obtained by offsetting HRMs, and the offset values can be shown in Fig. 13 and Table 7. For example, the method of HLE2 is

HRM2+0.1m which means the HLE can be obtained by offsetting HRM2 by 0.1m towards the right ("-" denotes left and "+" denotes right). The method of HLE3 is HRM3 which means the HLE can be obtained by using HRM3 directly without offsetting. From station K1+950.000 to station K2+260.000, the hard strip on the left side becomes wider. In this section, the HRM1 is replaced with HRM7 to form HRM1&7 together with the rest sections of HRM1. The HLE1 can be obtained by offsetting HRM1&7 by 0.1m towards the left. In most sections, the highway is a two-way four-lane highway. However, from the station of K0+473.999 to the station of K1+939.249, there are three lanes on the left side. In this section, Pj is constrained to HLE7 and VLE7, and in other sections, Pj is useless, which is constrained to HLE1 and VLE1 like Pg. In most highway sections, the distance between HHS1 and HLE5 (hard shoulder width) and the distance between HHS2 and HLE6 is 3.3m. However, in two bridge sections, the distance between HHS1 and HLE5 is narrower. Thus the HHS1 and HHS2 can be obtained by offsetting HLE5 and HLE6 towards left and right, respectively. And then, in some bridge sections, the position of HLE5 should be modified. According to Section 3.4, to obtain HVE1, HVE2, HST1, and HST2, E_{Hampel}-d and E'_{Hampel}-d per 10 stations from K0+050.000 to K6+327.668 should be calculated. The process and the result of E_{Hampel}-d, E'_{Hampel}-d and slope lines can be shown in Fig. 12, and the parameters can be shown in Table 6. In Fig. 12, the E'_{Hampel} values of red points are greater than 0.1 and E'_{Hampel} values of blue points are less than -0.1. Choose appropriate slope lines and their link edges to obtain HVE1, HVE2, HST1, HST2. Since the target highway is located in the plain area, and in most sections, the highway only has a single-level slope, digital twinning in this research only considers single-level slope modelling. After determining essential horizontal control lines, including HLEs, HHSs, HVEs, HSTs, the elevations of them can be obtained from the TIN. The elevations of HLEs, HHSs, HVEs should be filtered by Hampel filter and fitted by smoothing splines to get VLEs, VHSs, VVEs to assist in establishing a relatively smooth highway surface. However, VSTs can be obtained from the extracted elevation directly without filtering and fitting to describe the existing elevation of the sloop toes and to ensure the digital twin can fit the TIN. The filter and fit parameters can be shown in Table 7, where HAlignment and VAlignment denote horizontal and vertical alignment, respectively. HLE1 and VLE1, HLE3 and VLE3 can be combined to form 3D polylines, which are called 3DLE1 and 3DLE3, respectively. A new TIN called TIN2 can be established only using 3DLE1 and 3DLE3. Unlike other HLEs and VLEs, the elevations of HLE7 are obtained using a new method. For the sake of the digital twin model's continuity, the elevations of HLE7 are obtained from TIN2 to get VLE7. Thus, VLE7 is the interpolation of the VLE2 and VLE3 by the horizontal distance. Then an assembly can be established, and its points can be constrained to the corresponding horizontal and vertical control lines to make the highway digital twin. The pavement thickness of the assembly is 36cm which is set approximately and adequately according to the UK design manual [13]. The parameters and evaluation of the horizontal and vertical control lines and the digital twinning process can be expressed in Fig. 13 and Table 7. HST1 and HST2 are employed to hollow the TIN, and the aligned aerial photographs are attached to the hollowed TIN. The overall A1(M) digital twin consists of the highway digital twin and the hollowed TIN attached with aligned aerial photographs, as shown in Fig. 14. The overall highway digital twin is detachable and consists of different components such as central reserves, hard strips, lanes, hard shoulders, verges, and slopes that can be selected separately. Moreover, additional information can be added into the components as build information models such as IDs, stations, names, types, materials, etc. The highway digital twin in ifc and nwd format, including the highway, the hollowed terrain, and road markings, can be downloaded from:

https://drive.google.com/drive/folders/1izprrfHV225sHW6bt63nvz0WeaZ5O6NO?usp=sharing

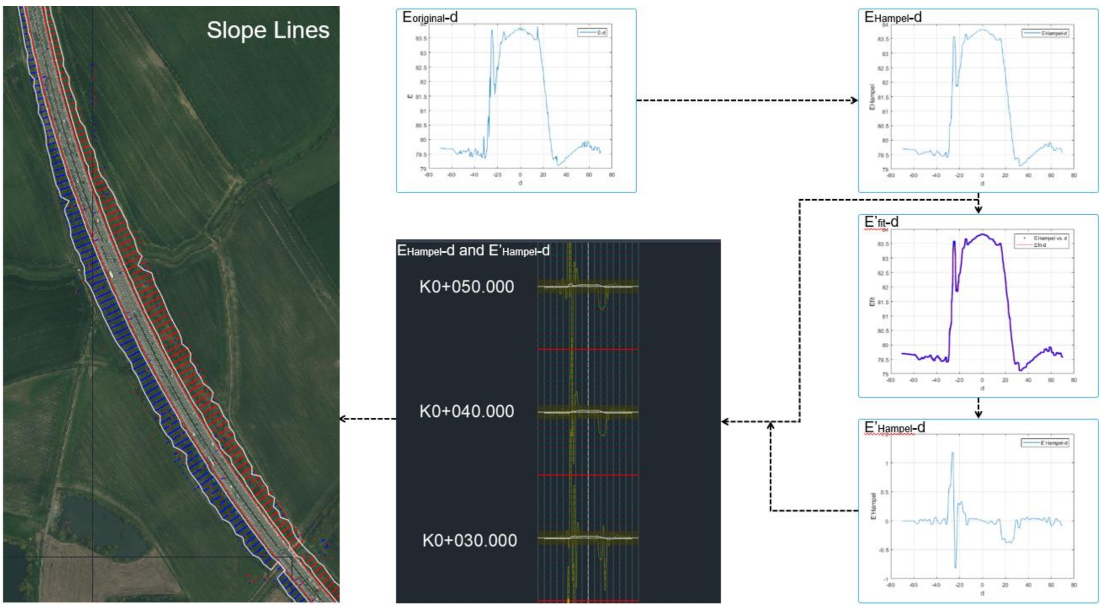

Fig. 12. Cross-section fitting and slope lines

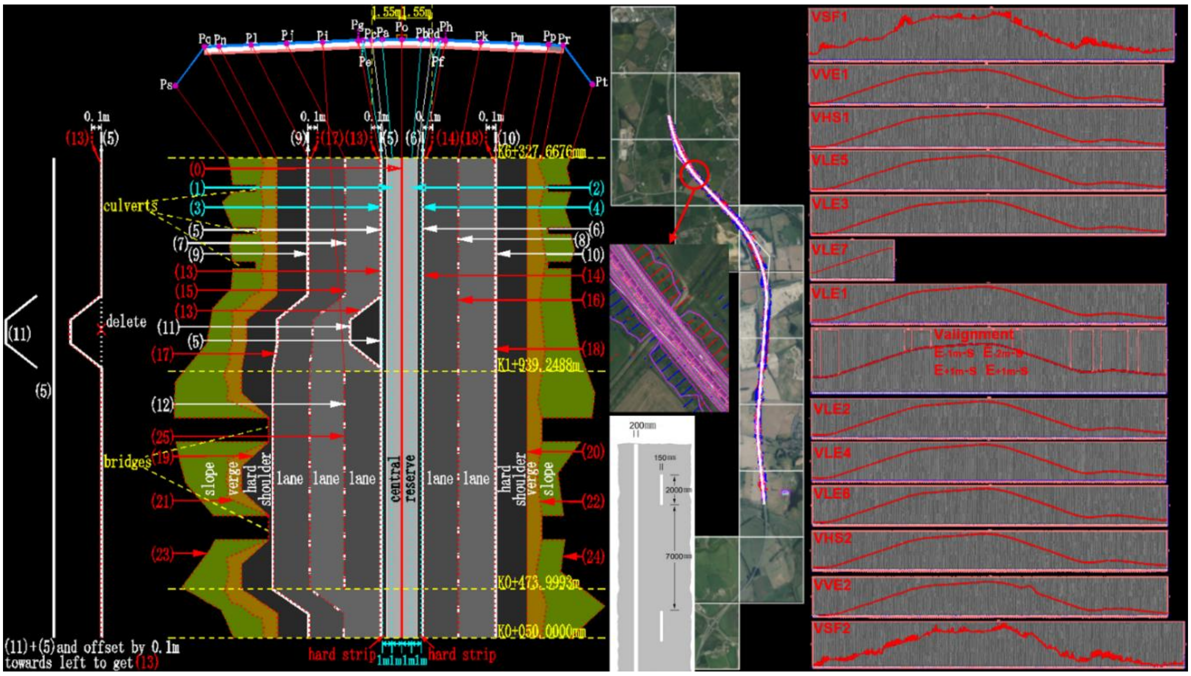

Fig. 13. The assembly of the road, constraints and modelling method

Table 6. Parameters of the cross-section processing

Name	Image in Fig. 12	Method	λ	RMSE	R-square	n	t
E_{Hampel}-d	ⓑ	Hampel filter				150	0.01
Efit-d	ⓒ	Smoothing spline fit	0.1	Various by stations	1		
E'_{Hampel}-d	ⓓ	Hampel filter				150	0.01

Table 7. Parameters and assignment of the constraints and their evaluation

No.	Position / Elevation	Constraint Point in Fig. 13	Method	n	t	λ	RMSE	R-square
(0)	HAlignment	Po	section3.2	-	-	section3.2	section3.2	section3.2
	VAlignment	Po	section3.3	150	0.1	1.6698E-06	0.00800	1
(1)	-1m	Pa	fixed value	-	-	-	-	-
	E-1m-s (fit)	Pa	hampel&fit	60	0.1	1.6698E-06	0.03995	1
(2)	+1m	Pb	fixed value	-	-	-	-	-
	E+1m-s (fit)	Pb	hampel&fit	60	0.1	1.6698E-06	0.04463	1
(3)	-2m	Pe	fixed value	-	-	-	-	-
	E-2m-s (fit)	Pe	hampel&fit	60	0.1	1.6698E-06	0.02558	1
(4)	+2m	Pf	fixed value	-	-	-	-	-
	E+2m-s (fit)	Pf	hampel&fit	60	0.1	1.6698E-06	0.02752	1
(5)	HRM1	-	fit	-	-	1.6700E-05	0.1593	1
	-	-	-	-	-	-	-	-
(6)	HRM2	-	fit	-	-	1.6700E-05	0.1662	1
	-	-	-	-	-	-	-	-
(7)	HRM3	-	fit	-	-	1.0000E-04	0.1408	1
	-	-	-	-	-	-	-	-
(8)	HRM4	-	fit	-	-	1.0000E-04	0.1519	1
	-	-	-	-	-	-	-	-

	HRM5	-	fit	-	-	1.0000E-04	0.1717	1
(9)	-	-	-	-	-	-	-	-
	HRM6	-	fit	-	-	1.0000E-04	0.1779	1
(10)	-	-	-	-	-	-	-	-
	HRM7	-	fit			1.0000E-05	0.1492	0.9999
(11)	-	-	-	-	-	-	-	-
	HRM8	-	fit			1.0000E-03	0.1859	0.9988
(12)	-	-	-	-	-	-	-	-
	HLE1	Pg	HRMS1&7-0.1	-	-	-	-	-
(13)	VLE1	Pg	hampel&fit	60	0.1	3.0000E-05	0.02257	1
	HLE2	Ph	HRMS2+0.1	-	-	-	-	-
(14)	VLE2	Ph	hampel&fit	60	0.1	3.0000E-05	0.02342	1
	HLE3	Pj	HRMS3	-	-	-	-	-
(15)	VLE3	Pj	hampel&fit	60	0.1	3.0000E-05	0.02589	1
	HLE4	Pk	HRMS4	-	-	-	-	-
(16)	VLE4	Pk	hampel&fit	60	0.1	3.0000E-05	0.02411	1
	HLE5	Pl	HRMS5+0.1	-	-	-	-	-
(17)	VLE5	Pl	hampel&fit	60	0.1	3.0000E-05	0.02532	1
	HLE6	Pm	HRMS6-0.1	-	-	-	-	-
(18)	VLE6	Pm	hampel&fit	60	0.1	3.0000E-05	0.03776	1
	HHS1	Pn	HLEP5-3.3m&modify	-	-	-	-	-
(19)	VHS1	Pn	hampel&fit	60	0.1	3.0000E-05	0.027689	1
	HHS2	Pp	HLEP6+3.3m&modify	-	-	-	-	-
(20)	VHS2	Pp	hampel&fit	60	0.1	3.0000E-05	0.02087	1
	HVE1	Pq	section3.4	-	-	-	-	-
(21)	VVE1	Pq	hampel&fit	60	0.1	3.0000E-05	0.07075	1
	HVE2	Pr	section3.4	-	-	-	-	-
(22)	VVE2	Pr	hampel&fit	60	0.1	3.0000E-05	0.08551	1
	HST1	Ps	section3.4	-	-	-	-	-
(23)	VST1	Ps	TIN	-	-	-	-	-
	HST2	Pt	section3.4	-	-	-	-	-
(24)	VST2	Pt	TIN	-	-	-	-	-
	HLE7	Pi	HRMS8	-	-	-	-	-
(25)	VLE7	Pi	TIN2	60	0.1	3.0000E-05	0.03204	1

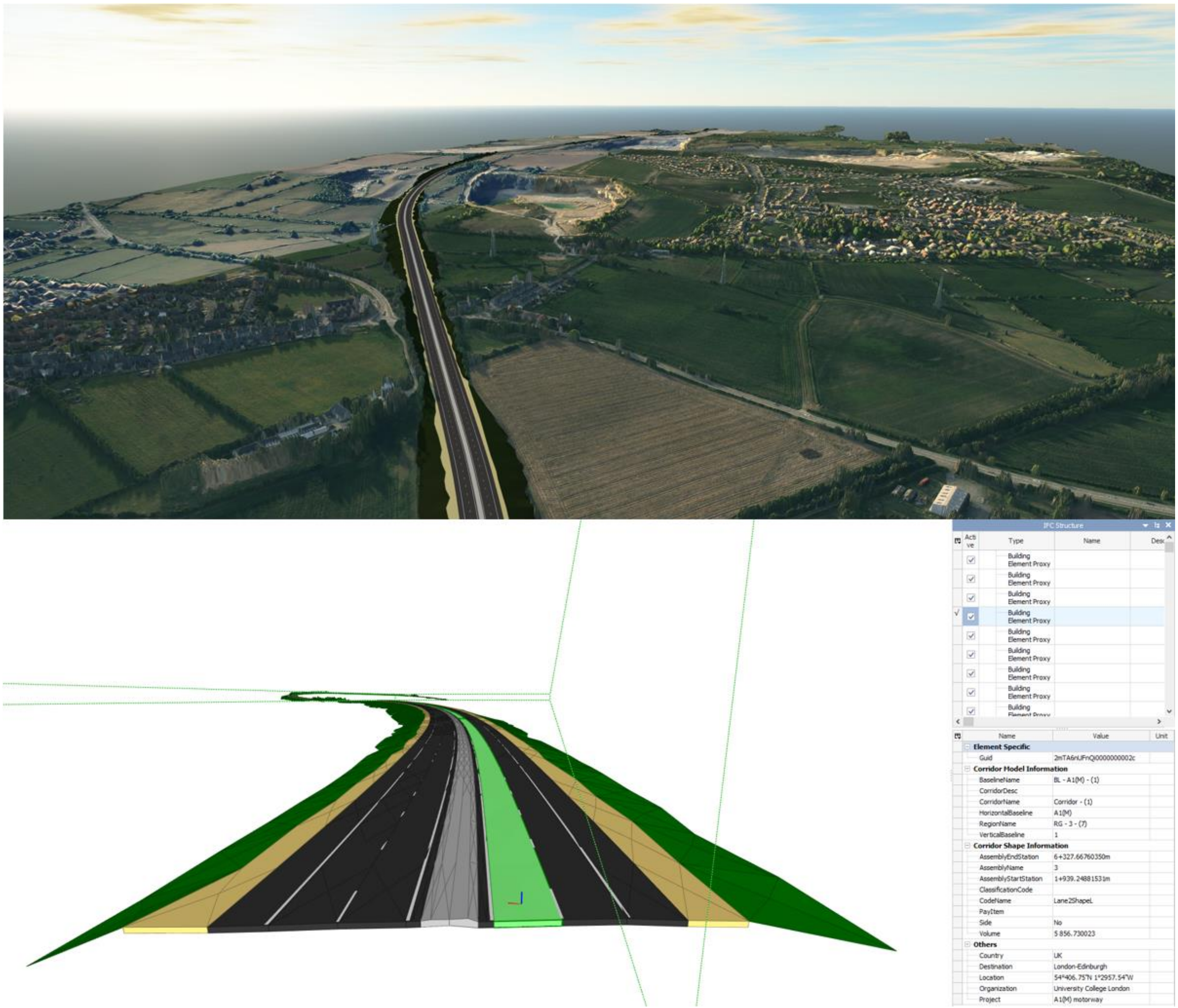

Fig. 14. The result of the highway digital twin and IFC format model with information

The original cross-section $E_{original}$-d is extracted directly from the TIN and the cross-section of the highway digital twin E_{DT}-d is obtained from the digital model. To evaluate the precision of the highway digital twin at every station, $E_{original}$-d and E_{DT}-d can be put in the same image. The start point, the endpoint, and the components' wide variations are shown in Fig. 15. The parameters of the highway digital twin's cross-sections at these stations are shown in Table 8. If the pavement descends from the alignment, the cross fall is positive and vice versa. In addition, to evaluate the highway digital twin's overall precision, HFT1 and HFT2 are combined into a closed polyline that can describe the horizontal scope of the highway digital twin considering side slopes. Similarly, HVE1 and HVE2 are combined into a closed polyline to describe the highway digital twin's horizontal scope without considering side slopes. In these two parts, the original DSM (DSM surface) and the top surface of the highway digital twin (DT surface) are extracted, respectively. No data areas are skipped. Afterwards, the volumes between the two surfaces are calculated. If the DT surface is below the DSM surface, the volume is expressed by V_{cut}. If the DT surface is above the DSM surface, the volume is expressed by V_{fill}. The horizontal areas of DSM surface are expressed by S. Thus, the highway digital twin's precision can be evaluated by Equation (17), where D denotes the average vertical deviation per square metre between the highway digital twin and the DSM. For the highway digital twin's precision considering side slopes, D_1= |93810.99791-41990.30716|/328901.82717=0.15756. For the highway digital twin's precision without considering side slopes, D_2= |17646.03140-4110.30243|/201197.50236=0.06728. The units of D_1 and D_2 are both metres. D_1 and D_2 provide a method to evaluate the highway digital twin. However, appropriate deviations from the DSM are acceptable because the proposed approach aims to infer a smoothing highway digital twin from map data and eliminate the influence of defects and fluctuations of the original data. Thus, appropriate deviations must exist.

$$D = \frac{|\sum V_{cut} - \sum V_{fill}|}{\sum S} \tag{17}$$

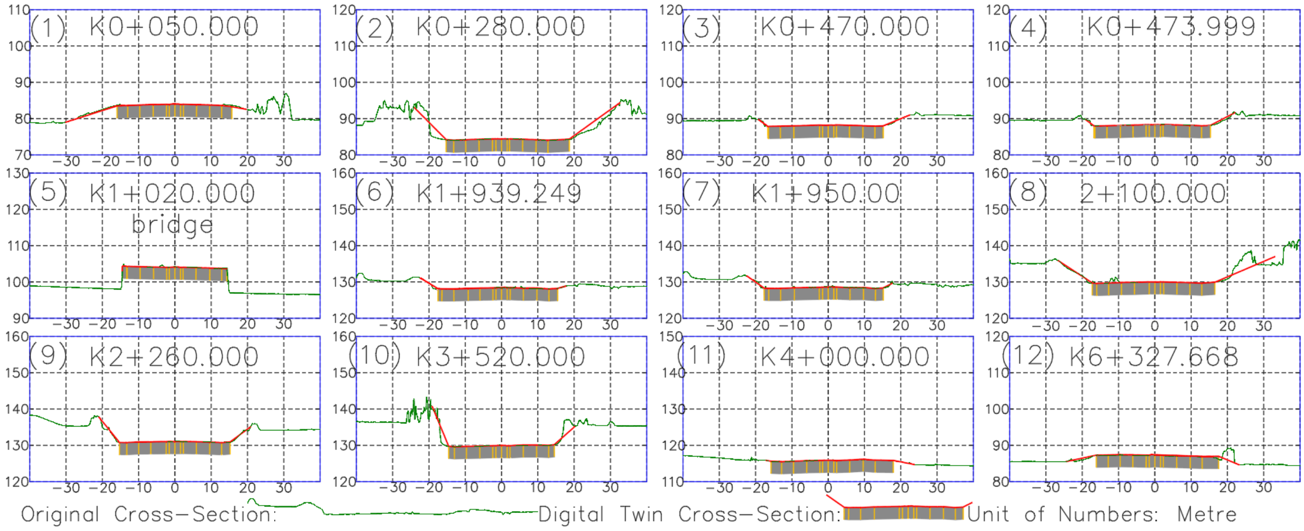

Fig. 15. The evaluation of the digital twin

Table 8. Parameters of typical cross-sections

station L: left R: right	**slop wide(m) /gradient cut:- fill:+**	**verge wide (m)**	**hard shoulder wide(m)**	**lane1 wide (m)**	**lane2 wide (m)**	**lane3 wide (m)**	**hard strip wide(m)**	**central reserve wide(m)**	**crossfall**
K0+050.000L	14.22/+32%	2.95	3.30	3.74	3.64	0.00	0.78	3.10	+3.1%
K0+050.000R	4.000/+18%	2.82	3.30	3.62	3.60	0.00	0.81		+2.9%
K0+280.000L	8.740/-100%	2.11	3.30	3.67	3.69	0.00	0.96	3.10	+3.1%
K0+280.000R	14.000/-72%	5.87	3.30	3.70	3.59	0.00	0.66		+3.5%
K0+470.000L	2.590/-71%	0.18	3.30	3.70	7.09	0.00	0.83	3.10	+2.6%
K0+470.000R	7.370/-40%	2.28	3.30	3.72	3.58	0.00	0.72		+3.5%
K0+473.999L	2.406/-74%	0.27	3.30	3.72	3.48	3.62	0.84	3.10	+2.6%
K0+473.999R	6.802/-52%	2.45	3.30	3.72	3.60	0.00	0.70		+3.5%
K1+020.000L	0.000(bridge)	1.25	0.10	3.56	3.71	3.60	0.73	3.10	-2.5%
K1+020.000R	0.000(bridge)	1.41	3.30	3.78	3.59	0.00	0.68		+3.0%
K1+939.249L	4.973/-60%	1.07	3.30	3.95	3.22	3.58	0.83	3.10	+2.3%
K1+939.249R	2.349/-29%	2.41	3.30	3.74	3.64	0.00	0.83		+3.0%
K1+950.000L	4.827/-70%	1.23	3.30	3.79	6.85	0.00	0.91	3.10	+2.3%
K1+950.000R	2.490/-50%	2.13	3.30	3.72	3.67	0.00	0.80		+3.0%
K2+100.000L	9.460/-66%	1.24	3.30	3.52	3.59	0.00	4.05	3.10	+2.7%
K2+100.000R	16.590/-43%	3.59	3.30	3.56	3.66	0.00	0.89		+3.1%
K2+260.000L	5.670/-123%	2.00	3.30	3.35	4.21	0.00	0.87	3.10	+2.2%
K2+260.000R	5.630/-74%	2.32	3.30	3.66	3.58	0.00	0.79		+3.0%
K3+520.000L	4.540/-242%	1.60	3.30	3.68	3.56	0.00	0.88	3.10	+2.9%
K3+520.000R	5.760/-88%	1.57	3.30	3.69	3.66	0.00	0.78		-0.8%
K4+000.000L	1.490/-17%	2.90	3.30	3.64	3.61	0.00	0.75	3.10	+3.3%
K4+000.000R	5.890/+20%	5.00	3.30	3.72	3.58	0.00	0.80		-1.6%
K6+327.668L	8.320/+21%	3.27	3.30	3.48	3.69	0.00	0.83	3.10	-0.6%
K6+327.668R	5.689/+42%	4.53	3.30	3.73	3.68	0.00	0.79		+2.9%

5 DISCUSSION

From the perspective of the target projects, this paper provides an effective digital twinning approach for an existing highway which is a long-shape transportation infrastructure and adheres to the terrain ups and downs. In this kind of existing project, people should consider not only the structure (BIM) but also the surroundings (GIS). A highway can be regarded as a structure as well as a part of the environment. Also, in the digital twinning process, the existing highway defects such as cracking, rutting, potholes, slab staggering, side slope erosion, blurred components' boundaries, etc., should be considered. Moreover, the surroundings' influences, such as the shelter from the trees, overpasses, and other surrounding projects, should also be considered. The proposed approach can be implemented in similar highway projects.

From the perspective of digital twinning, The proposed method is advanced in the following aspects. a) outliers on the original map data can be easily removed to enhance the quality of the data; b)an accurate and smooth digital twin model (the average vertical deviation per square metre between the surface of the generated digital twin and the actual data was at the centimetre level) can be generated using the map data without field surveys and design documents; c)the highway digital twin conforms to the representation habits of highway engineering, and some parameters of the highway can be inferred; d)the digital twin consists of primary highway components, such as horizontal alignment, vertical alignment, lanes, central reserves, hard strips, hard shoulders, verges, and side slopes which were not distinguished in other methods.

From the perspective of connections between the physical project and the digital twin, there are no devices employed directly by this research for the digital twinning, and the data is just from the existing map database. However, the map data may be collected by satellites, airborne LiDAR, and more in the past, which can be regarded as the connections between the physical project and the digital twin.

From the perspective of the data resources, some issues should be discussed. Firstly, the map data can be obtained through different map data downloading platforms flexibly, such as NASA EOS, Map World, Digimap, ESA, GeoEye, Google Map, Google Earth, Bing Maps, OpenStreetMap, ArcGIS, Baidu Map, BIGEMAP, MapBox, etc. According to the different locations of the target projects, different purposes of the research, different demands of the data accuracy, and data types, people should choose appropriate map platforms. Besides, different platforms can be leveraged together to complement each other according to their strengths and weaknesses. Secondly, unlike the field survey, which can collect different data from different angles and at different positions according to demands, the map's data are usually collected from the top. Thus, the shelter of the overpasses, vehicles and other objects should be considered, and the proposed approach has solved this issue. Thirdly, the defects caused by the low quality of the downloaded data are also considered in this paper.

From the perspective of the applications, the digital twin of the existing old highway using existing map data has the potential to be implemented in highway network planning, highway O&M, traffic simulation and analysis, reconstruction and expansion, etc.

Simultaneously, the implementation of the proposed approach has some limitations. First, the proposed approach has only been implemented in the plan areas and only makes digital twins considering the single-level side slopes. In mountainous areas, a highway has multi-level side slopes. Actually, the slope lines of multi-level side slopes and the berms between slopes have been outlined, as it is mention in Section 3.4. Second, due to the limitation of the data's quality, side ditches are too blurry to be identified, and this paper does not consider digital twinning for side ditches.

6 CONCLUSIONS

A novel approach has been proposed for generating the digital twin of a highway using map data based on road engineering expertise, including data acquisition and processing, horizontal alignment fitting, vertical alignment fitting, cross-section processing, and digital twinning. The proposed approach has been successfully implemented in a section of the A1(M) motorway in the UK, and the highway digital twin has been evaluated. The data is readily available without a field survey, the digital twin is in accordance with the expression of road engineering, and it has good accuracy.

There are some contributions that this article can bring to the field:

1) This paper presents a systematic digital twinning method for existing old highways considering different highway components and the relationship with the terrain (side slope).

2) Using the proposed approach, the data resources are existing online map data, which are pretty available. This approach allows some research and work related to highways using digital twins not to be restricted by the field survey and exceptional circumstances.

3) This paper provides a method to reduce the influence of the defects, outliers and spikers on digital twin caused by the old highway and the low quality of the downloaded map data.

4) The digital twinning process is from the perspective of road engineering expertise; thus, the highway digital twin is in accordance with the engineering expression of the highway.

Several aspects will be considered in further research:

1) The proposed method was implemented on a highway in plain areas. In addition, this research only considered the first-level side slopes. However, some highways are built in mountainous areas with multi-level side slopes and berms, which will be considered in future research.

2) The proposed method was implemented using aerial photography, DSM data, topography from Digimap in the UK. There is a lack of imagery data for highways in many other countries, which will be considered in future research.

ACKNOWLEDGMENTS

This study is supported by Major Science &Technology Project of Hubei (Grant No. 2020ACA006)

REFERENCES

[1] LiDAR Digimap Help, https://digimap.edina.ac.uk/webhelp/lidar/lidardigimaphelp.htm#copyright/licence_agreement.htm.

[2] G. Angjeliu, D. Coronelli, G. Cardani, Development of the simulation model for Digital Twin applications in historical masonry buildings: The integration between numerical and experimental reality, Computers and Structures 238 (2020).

[3] M.R.M.F. Ariyachandra, I. Brilakis, Detection of Railway Masts in Airborne LiDAR Data, Journal of Construction Engineering and Management 146 (9) (2020).

[4] S. Biçici, M. Zeybek, An approach for the automated extraction of road surface distress from a UAV-derived point cloud, Automation in Construction 122 (2021).

[5] C. Boje, A. Guerriero, S. Kubicki, Y. Rezgui, Towards a semantic Construction Digital Twin: Directions for future research, Automation in Construction 114 (2020).

[6] J. Böke, U. Knaack, M. Hemmerling, Prototype of a cyber-physical façade system, Journal of Building Engineering 31 (2020).

[7] F.J. Camacho-Torregrosa, A.M. Pérez-Zuriaga, J.M. Campoy-Ungría, A. García, A.P. Tarko, Use of heading direction for recreating the horizontal alignment of an existing road, Computer-Aided Civil and Infrastructure Engineering 30 (4) (2015) 282-299.

[8] J.C.P. Cheng, Q. Lu, Y. Deng, Analytical review and evaluation of civil information modeling, Automation in Construction 67 (2016) 31-47.

[9] Digimap, https://digimap.edina.ac.uk/lidar.

[10] S.M. Easa, F. Wang, Estimating continuous highway vertical alignment using the least-squares method, Canadian Journal of Civil Engineering 37 (10) (2010) 1362-1370.

[11] H. England, CD 109 - Highway link design, Design Manual for Roads and Bridges, Highways England, United Kingdom, 2020.

[12] H. England, CD 127 - Cross-sections and headrooms, Design Manual for Roads and Bridges, Highways England, United Kingdom, 2020.

[13] H. England, CD 226 - Design for new pavement construction, Design Manual for Roads and Bridges, Highways England, United Kingdom, 2020.

[14] H. England, CG 501 - Design of highway drainage systems, Design Manual for Roads and Bridges, Highways England, United Kingdom, 2020.

[15] L. Garach, J. De Oña, M. Pasadas, Determination of alignments in existing roads by using spline techniques, Mathematics and Computers in Simulation 102 (2014) 144-152.

[16] M. Grieves, J. Vickers, Digital twin: Mitigating unpredictable, undesirable emergent behavior in complex systems, Transdisciplinary Perspectives on Complex Systems: New Findings and Approaches, Springer International Publishing, 2016, pp. 85-113.

[17] A. Holgado-Barco, B. Riveiro, D. González-Aguilera, P. Arias, Automatic Inventory of Road Cross-Sections from Mobile Laser Scanning System, Computer-Aided Civil and Infrastructure Engineering 32 (1) (2017) 3-17.

[18] D. Huynh, S. Nguyen-Ky, Engaging Building Automation Data Visualisation Using Building Information Modelling and Progressive Web Application, Open Engineering 10 (1) (2020) 434-442.

[19] O.Z. Jasim, Using of machines learning in extraction of urban roads from DEM of LIDAR data: Case study at Baghdad expressways, Iraq, Periodicals of Engineering and Natural Sciences 7 (4) (2019) 1710-1721.

[20] S. Kaewunruen, N. Xu, Digital twin for sustainability evaluation of railway station buildings, Frontiers in Built Environment 4 (2018).

[21] A. Karamanou, K. Papazissi, D. Paradissis, B. Psarianos, Precise estimation of road horizontal and vertical geometric features using mobile mapping techniques, Boletim de Ciencias Geodesicas 15 (5) (2009) 762-775.

[22] W. Kritzinger, M. Karner, G. Traar, J. Henjes, W. Sihn, Digital Twin in manufacturing: A categorical literature review and classification, 15th IFAC Symposium on Information Control Problems in Manufacturing, INCOM 2015 51 (11) (2018) 1016-1022.

[23] K. Lin, Y.L. Xu, X. Lu, Z. Guan, J. Li, Digital twin-based collapse fragility assessment of a long-span cable-stayed bridge under strong earthquakes, Automation in Construction 123 (2021).

[24] L. Liu, S. Lim, Color component-based road feature extraction from airborne lidar and imaging data sets, Journal of Surveying Engineering 143 (1) (2017).

[25] Z. Liu, W. Bai, X. Du, A. Zhang, Z. Xing, A. Jiang, Digital Twin-based Safety Evaluation of Prestressed Steel Structure, Advances in Civil Engineering 2020 (2020).

[26] C. Llorca, A. García, Evaluation of passing process on two-lane rural highways in spain with new methodology based on video data, Transportation Research Record, 2011, pp. 42-51.

[27] Q. Lu, L. Chen, S. Li, M. Pitt, Semi-automatic geometric digital twinning for existing buildings based on images and CAD drawings, Automation in Construction 115 (2020).

[28] R. Lu, I. Brilakis, Digital twinning of existing reinforced concrete bridges from labelled point clusters, Automation in Construction 105 (2019).

[29] X. Lü, C. Cheng, J. Gong, L. Guan, Review of data storage and management technologies for massive remote sensing data, Science China Technological Sciences 54 (12) (2011) 3220-3232.
[30] G.P. Lydon, S. Caranovic, I. Hischier, A. Schlueter, Coupled simulation of thermally active building systems to support a digital twin, Energy and Buildings 202 (2019).
[31] MathWorks, Smoothing Splines, in: MathWorks (Ed.), MathWorks, MathWorks, MathWorks, 2020.
[32] M. Omer, L. Margetts, M. Hadi Mosleh, S. Hewitt, M. Parwaiz, Use of gaming technology to bring bridge inspection to the office, Structure and Infrastructure Engineering 15 (10) (2019) 1292-1307.
[33] R.K. Pearson, Y. Neuvo, J. Astola, M. Gabbouj, Generalized Hampel Filters, Eurasip Journal on Advances in Signal Processing 2016 (1) (2016).
[34] Y. Peng, M. Zhang, F. Yu, J. Xu, S. Gao, Digital Twin Hospital Buildings: An Exemplary Case Study through Continuous Lifecycle Integration, Advances in Civil Engineering 2020 (2020).
[35] A. Ragnoli, M.R. De Blasiis, A. Di Benedetto, Pavement distress detection methods: A review, Infrastructures 3 (4) (2018).
[36] C. Rausch, C. Haas, Automated shape and pose updating of building information model elements from 3D point clouds, Automation in Construction 124 (2021).
[37] T.G. Ritto, F.A. Rochinha, Digital twin, physics-based model, and machine learning applied to damage detection in structures, Mechanical Systems and Signal Processing 155 (2021).
[38] R. Rosen, G. Von Wichert, G. Lo, K.D. Bettenhausen, About the importance of autonomy and digital twins for the future of manufacturing, 15th IFAC Symposium on Information Control Problems in Manufacturing, INCOM 2015 28 (3) (2015) 567-572.
[39] L.S. Shen, G.Q. Yang, H.T. Cheng, R.J. Zheng, J.C. Chen, Optimisation technology for geogrid-reinforced subgrade widening projects of highways, Yantu Gongcheng Xuebao/Chinese Journal of Geotechnical Engineering 35 (4) (2013) 789-793.
[40] C.S. Shim, N.S. Dang, S. Lon, C.H. Jeon, Development of a bridge maintenance system for prestressed concrete bridges using 3D digital twin model, Structure and Infrastructure Engineering 15 (10) (2019) 1319-1332.
[41] W. Tao, B. Cai, J. Wang, J. Liu, W. Shangguan, Research on Geometry Extraction of Railway Horizontal Curves for Digital Track Map, Tiedao Xuebao/Journal of the China Railway Society 41 (9) (2019) 81-87.
[42] D.f. Transport, Chapter 5 Road Markings, Traffic Signs Manual, Highways England, United Kingdom, 2018.
[43] E.J. Tuegel, A.R. Ingraffea, T.G. Eason, S.M. Spottswood, Reengineering aircraft structural life prediction using a digital twin, International Journal of Aerospace Engineering (2011).
[44] Y. Wei, B. Akinci, A vision and learning-based indoor localisation and semantic mapping framework for facility operations and management, Automation in Construction 107 (2019).
[45] Wikipedia, List of countries by road network size, Wikipedia, 2021.
[46] X. Xie, Q. Lu, D. Rodenas-Herraiz, A.K. Parlikad, J.M. Schooling, Visualised inspection system for monitoring environmental anomalies during daily operation and maintenance, Engineering, Construction and Architectural Management 27 (8) (2020) 1835-1852.
[47] Y.F. Yang, Technological methods of environmental evaluation for highway network planning, Journal of Traffic and Transportation Engineering 6 (1) (2006) 113-117.
[48] S. Ye, X. Lai, I. Bartoli, A.E. Aktan, Technology for condition and performance evaluation of highway bridges, Journal of Civil Structural Health Monitoring 10 (4) (2020) 573-594.
[49] G. Yu, S. Zhang, M. Hu, Y. Ken Wang, Prediction of highway tunnel pavement performance based on digital twin and multiple time series stacking, Advances in Civil Engineering 2020 (2020).
[50] H. Zhang, J. Wei, X. Zhang, Comparative Study on Road Plane Alignment Fitting Methods, Wuhan Ligong Daxue Xuebao (Jiaotong Kexue Yu Gongcheng Ban)/Journal of Wuhan University of Technology (Transportation Science and Engineering) 42 (4) (2018) 594-598 and 603.